Vilniaus universiteto
Fizikos fakulteto
Fotonikos ir nanotechnologijų institutas

Aistė Štaupienė

ATKAITINTŲ GaAsBi/AlGaAs PARABOLINIŲ KVANTINIŲ DUOBIŲ SU SUSIFORMAVUSIAIS Bi KVANTINIAIS TAŠKAIS OPTINIS TYRIMAS

Magistrantūros studijų baigiamasis darbas

Fotonikos ir nanotechnologijų
studijų programa

Studentas	Aistė Štaupienė
Leista ginti	2026-05-20
Darbo vadovas	dr. Evelina Dudutienė
Instituto direktorius	prof. dr. Ramūnas Aleksiejūnas

Vilnius 2026

Vilnius University
Faculty of Physics

Aistė Štaupienė

OPTICAL INVESTIGATION OF ANNEALED GaAsBi/AlGaAs PARABOLIC QUANTUM WELLS WITH Bi QUANTUM DOTS

Master's final thesis
Photonics and Nanotechnology study programme

Student	Aistė Štaupienė
Approved	2026-05-20
Academic Supervisor	Dr. Evelina Dudutienė
Director of the Institute	Prof. Dr. Ramūnas Aleksiejūnas

Vilnius 2026

Table of Contents

Abbreviations **4**

Publications **5**

Introduction **7**

1 Literature review **8**

1.1 GaAsBi structures 8

1.2 GaAsBi growth 9

1.3 Bi quantum dots 10

1.4 Optical properties of bismides 11

2 Experimental methodology **13**

2.1 Sample growth 13

2.2 Transmission electron microscopy 15

2.3 Cathodoluminescence measurements 15

2.4 Photoluminescence measurements 16

3 Results **17**

3.1 Annealing treatments 17

3.1.1 Structural changes 17

3.1.2 Optical properties 19

3.2 Dot-in-a-well structure 24

3.2.1 Emission properties 24

3.3 Structures with ultrathin AlAs barriers 28

3.3.1 Size control of Bi quantum dots 28

3.3.2 Effect on GaAsBi quantum wells 30

Conclusions **35**

References **36**

Summary **41**

Santrauka **43**

Abbreviations

CB	Conduction Band
CL	Cathodoluminescence
DWELL	Dot-in-a-Well
DPSS	Diode-Pumped Solid-State
EDX	Energy-Dispersive X-ray
HAADF	High-Angle Annular Dark-Field
HT	High-Temperature
LD	Laser Diode
LED	Light Emitting Diode
LT	Low-Temperature
LTCL	Low-Temperature Cathodoluminescence
LTPL	Low-Temperature Photoluminescence
MBE	Molecular Beam Epitaxy
NIR	Near-Infrared
PL	Photoluminescence
PQW	Parabolic Quantum Well
QD	Quantum Dot
QW	Quantum Well
RT	Room-Temperature
RTPL	Room-Temperature Photoluminescence
STEM	Scanning Transmission Electron Microscopy
TEM	Transmission Electron Microscopy
TDPL	Temperature-Dependent Photoluminescence
VB	Valence Band

Publications

The study of annealed GaAsBi/AlGaAs parabolic quantum wells was published in 2 scientific papers and 7 conference reports (excluding co-authored reports). Some of the publications were made under the author's maiden name (A. Butkutė).

Scientific papers:

- **A. Štaupienė**, M. Jokubauskaitė, A. Zelioli, A. Špokas, M. Skapas, B. Čechavičius, R. Butkutė, E. Dudutienė. Improving optical properties through growth temperatures and post-growth annealing in parabolic GaAsBi/AlGaAs quantum wells. *Journal of Alloys and Compounds*, 1060, 187230 (2026).
- E. Dudutienė, **A. Štaupienė**, A. Špokas, A. Zelioli, B. Čechavičius, R. Butkutė. Influence of growth temperature and post-growth annealing on optical emission from GaAsBi/AlGaAs double parabolic quantum well structures. *Proc. SPIE 13582, Low-Dimensional Materials and Devices 2025*, 135820F (2025).

Conference reports:

- **A. Štaupienė**, A. Zelioli, A. Špokas, M. Skapas, B. Čechavičius, R. Butkutė, E. Dudutienė. Structural and Optical Investigation of GaAsBi/AlGaAs Parabolically Graded Quantum Well Structures. 69th international conference for students of physics and natural sciences "Open readings 2026", Vilnius, Lithuania, 27 – 30 April, 2026. (oral presentation)
- **A. Štaupienė**, M. Jokubauskaitė, A. Špokas, A. Zelioli, S. Stanionytė, B. Čechavičius, R. Butkutė, E. Dudutienė. GaAsBi QW emisijos intensyvumo stiprinimas panaudojant AlGaAs gradientinius barjerus bei struktūrų atkaitinimą. 46-oji Lietuvos Nacionalinė fizikos konferencija "LNFK2025", Kaunas, Lithuania, 8 – 10 October, 2025. (poster presentation)
- **A. Štaupienė**, M. Jokubauskaitė, A. Špokas, A. Zelioli, S. Stanionytė, B. Čechavičius, R. Butkutė, E. Dudutienė. Improved Emission Properties of GaAsBi QWs Due AlGaAs Graded Barrier Design and Thermal Annealing. 15-oji FTMC PhD Students and Young Researchers Conference "FizTeCh2025", Vilnius, Lithuania, 21 – 22 October, 2025. (poster presentation)
- **A. Štaupienė**, E. Dudutienė. Atkaitintų GaAsBi kvantinių duobių su paraboliniais AlGaAs barjerais optinių savybių tyrimas. Studentų mokslinė konferencija „Naujoji karta su LMT", Vilnius, Lithuania, 22 May, 2025. (oral presentation)
- **A. Štaupienė**, A. Špokas, A. Zelioli, B. Čechavičius, R. Butkutė, E. Dudutienė. Photoluminescence investigation of the annealing effects on GaAsBi quantum wells with parabolic AlGaAs barriers. 22nd Euro MBE Workshop "EuroMBE 2025", Auron, France, 9 – 13 March, 2025. (poster presentation)

- **A. Butkutė**, M. Jokubauskaitė, A. Špokas, A. Zelioli, B. Čechavičius, E. Dudutienė, R. Butkutė. Optical Properties of InGaAs and GaAsBi Quantum Wells with Graded AlGaAs Barriers. 52nd International School & Conference on the Physics of Semiconductors, Szczyrk, Poland, 15 – 21 June, 2024. (poster presentation)
- **A. Butkutė**, M. Jokubauskaitė, A. Špokas, A. Zelioli, B. Čechavičius, S. Stanionytė, R. Butkutė, E. Dudutienė. The influence of graded AlGaAs barriers on optical properties of GaAsBi single quantum wells. Workshop "European Workshop on Innovative and Advanced Epitaxy – OPERA", Vilnius, Lithuania, June 11 – 14, 2024. (oral presentation)

Introduction

Gallium arsenide bismide quantum well (QW) structures are one category of materials currently being studied for active area of light sources operating in the near-infrared (NIR) range [1]. GaAsBi exhibits a low bandgap energy sensitivity to temperature [2], a pronounced bandgap reduction with increasing bismuth incorporation [3] and the potential to suppress non-radiative Auger-Meitner recombination mechanisms [4].

However, complicated growth conditions of bismides [5], lead to reduced GaAsBi crystal quality and increased point defect density [6]. This has a detrimental effect on emission efficiency [7] and therefore limits the practical implementation of GaAsBi-based structures in optoelectronic devices.

Thus, various technological modifications [8-14] are being explored to minimize defect density and enhance emission intensity. For example, implementing separate confinement heterostructures (SCH) increases emission intensity [8], owing to enhanced carrier confinement and trapping efficiency [9]. Additionally, thermal treatments can be employed to decrease the density of non-radiative recombination centers and alloy disorder [10-14]. Annealing can also induce Bi redistribution and formation of Bi quantum dots (QDs), which, when controlled to optimal dimensions, can emit in the 1300 – 1500 nm spectral range relevant for telecommunication technologies [15]. However, this Bi migration process can also distort the quantum structure by degrading its heterointerfaces. Therefore, to obtain high-quality heterostructures the segregation of Bi should be suppressed. This can be addressed by introducing Al-containing barriers, which act as an effective Bi-blocking layers, limit unwanted Bi diffusion out of GaAsBi [16] and additionally allow to control the size of Bi QDs formed in the QW [17, 18].

This work aims to study how thermal treatments and barrier design affect the emission and structural properties of GaAsBi/AlGaAs parabolic quantum well (PQW) structures with Bi QDs.

To achieve the aim of this thesis, the following tasks were set:

- Investigate optical performance of GaAsBi PQW structures using room-temperature, temperature-dependent and excitation-dependent photoluminescence techniques.
- Evaluate structural and optical changes induced by *in-situ* and *ex-situ* annealing in GaAsBi PQW structures.
- Verify and study Bi QD emission properties using photoluminescence and cathodoluminescence measurements.
- Determine optical performance trends linked to formation of ultrathin AlAs barriers.

1 Literature review

This chapter outlines main properties of GaAsBi quantum structures, including their growth and possible technological modifications for improved optical performance, which can be investigated with presented optical analysis methods.

1.1 GaAsBi structures

GaAsBi is currently under investigation as potential NIR emitter. It possesses unique optical and electronic characteristics distinct from other conventional materials. The incorporation of Bi reduces the bandgap of GaAsBi by 60 – 90 meV per %Bi [3, 19, 20], making it a promising candidate for NIR emitters. Strong spin-orbit splitting is also induced by Bi incorporation into the GaAs lattice. Once the Bi concentration exceeds 10.5 %, the spin-orbit splitting energy becomes larger than the bandgap, which can reduce Auger-Meitner recombination and inter-valence band absorption [4]. These processes are the main efficiency loss sources in InGaAsP lasers used for the telecommunications [21]. Additionally, the bandgap of GaAsBi has high thermal stability (see Fig. 1.1) [2, 22]. Such properties are essential for developing stable optoelectronic devices that can operate without additional cooling, making GaAsBi QW structures attractive for lasers [23, 24] and other emitters [25, 26].

First GaAsBi light emitting diode (LED), containing 50 nm thick GaAsBi active layer with 1.8 % of Bi, was demonstrated in 2009 [25]. One year later, Tominaga *et al.*, reported the first optically pumped GaAsBi laser, which emitted at 982.8 nm from a 390 nm GaAsBi layer containing 2.5% Bi [24]. This device also exhibited a two times smaller temperature coefficient of the lasing emission peak energy compared to GaAs.

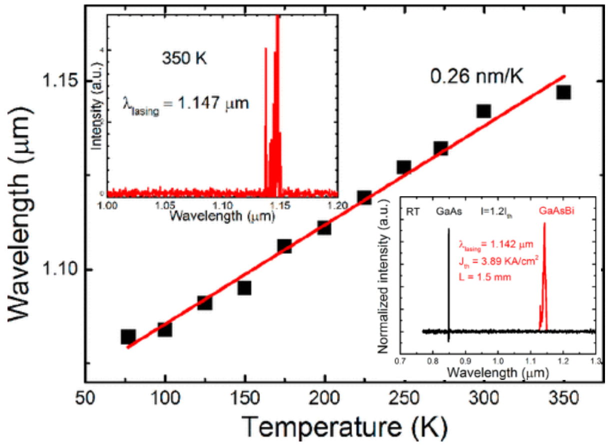

Fig. 1.1. GaAsBi QW laser wavelength dependence on temperature. Insets show lasing spectra at RT and 350 K. Taken from [22].

In 2013, the first electrically driven GaAsBi laser diode (LD) was demonstrated, with an active area containing 2.2% of Bi and emission around 947 nm [26]. A year later, Butkutė *et al*. reported a multi-quantum well device consisting of three 8-nm QWs with 6.5% Bi that operated at 1060 nm. [27]. The longest emission wavelength reported for GaAsBi QW edge-emitting laser at RT is 1142 nm, demonstrated in 2017 (Fig. 1.1) [22].

Thus, it can be observed that progress in GaAsBi research has led to an increase in Bi incorporation and a corresponding shift of emission toward longer, NIR wavelengths.

1.2 GaAsBi growth

Although GaAsBi emitters have been demonstrated [22-27], their fabrication remains challenging due to the difficulties in the epitaxial growth of Bi-containing layers, which often limits the optical quality required for practical device applications. This is because the growth of GaAsBi quantum structures requires low temperatures (≤ 440 °C), well below the optimal GaAs growth temperature, to enable the incorporation of large Bi atoms into the GaAs lattice [5]. This leads to high density of defects and reduced crystalline quality, resulting in a significant quenching of GaAsBi luminescence intensity [6] and milli-percent emission efficiency [7], necessitating the employment of growth optimization and technological modification techniques in order to improve GaAsBi structural quality and enhance internal quantum efficiency, for it to function as efficient emitter.

Fortunately, various process adjustments used to enhance structural and optical properties of GaAsBi structures have been thoroughly researched and are already employed in molecular beam epitaxy (MBE) growth. For example, stoichiometric As_2/Ga flux ratios are favoured for the most efficient Bi incorporation [5] and reduced surface roughness [28], while two substrate temperature growth , where Bi containing layers are grown at lower temperature, which is later increased for the growth of barriers, is employed to improve crystalline quality of the structures [29, 30].

Technological measures, like rapid thermal annealing [10-14] or separate confinement heterostructures [8, 9] also can be incorporated into GaAsBi growth processes to improve material quality and optical response.

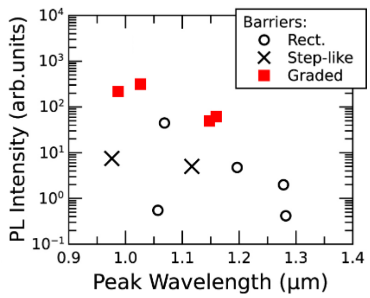

Fig. 1.2. Photoluminescence intensity dependence on peak wavelength for GaAsBi QW structures with different barrier designs. Taken from [8].

Implementing SCH, for example, GaAsBi quantum wells with parabolically graded AlGaAs barriers, increases emission intensity, compared to conventional structures (see Fig. 1.2) [8], owing to enhanced carrier confinement and trapping efficiency [9]. Moreover, the use of parabolically graded barriers can enhance LD performance by increasing its maximum output powers and decreasing threshold currents [31].

Thermal annealing can be performed either in the MBE reactor (*in-situ*) or in a rapid thermal annealing (RTA) furnace (*ex-situ*). This technique is highly temperature and structure-dependent, meaning that precise temperature control is needed to prevent Bi diffusion and defect formation [14, 32]. However, when optimized, thermal treatments can decrease non-radiative recombination centers [10, 11] and alloy disorder [13], enhance emission intensities [12, 14] or even form Bi QDs in GaAsBi layers [15-18].

1.3 Bi quantum dots

Bi clustering to QDs induced by thermal treatments is being extensively researched as an alternative route toward bismide-based NIR emitters [33]. Bismuth nanocrystals become semiconducting once their diameter drops below 16 nm, however reducing their size to 8 – 10 nm creates 0D structures that can emit at 1.30 – 1.55 μm [15], making them attractive for telecom applications. Therefore, control of the QD size is extremely important. One approach for it is to anneal GaAsBi quantum wells with a high concentration of Bi to promote QD formation inside the well, creating a dot-in-a-well (DWELL) structure (Fig. 1.3). This way the width of QW can influence the resulting diameter of QDs [17, 18].

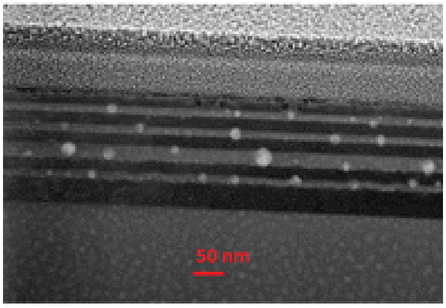

Fig. 1.3. Transmission electron microscopy image of GaAsBi/AlAs DWELL structure. Taken from [15].

However, annealing often degrades the heterostructures due to bismuth interlayer migration and segregation toward the surface [15]. Additionally, resulting emission from such DWELL structures can be broad due to the wide QD size distribution and therefore overlapped emissions [34, 35].

Therefore, to improve the structural and optical quality, Bi migration process should be suppressed within the GaAsBi QW. This can be addressed by introducing Al-containing barriers [15-17], such as AlGaAs barriers or ultrathin AlAs layers between the QW and the barrier. These Al-containing layers act as an effective Bi-blocking barriers, limit unwanted Bi diffusion [16] and help to control the size of Bi QDs formed in the QW [17, 18].

1.4 Optical properties of bismides

Optical properties of GaAsBi QWs or Bi QDs is typically studied by photoluminescence (PL) technique. Here photoexcited electrons relax from conduction band (CB) and recombine with holes in the valence band (VB) producing luminescence (Fig. 1.4). This PL is used for analysing emission spectra, peak position (approximately corresponds to the bandgap energy), the redshift rate of the bandgap, carrier localization effect and carrier recombination processes [36, 37].

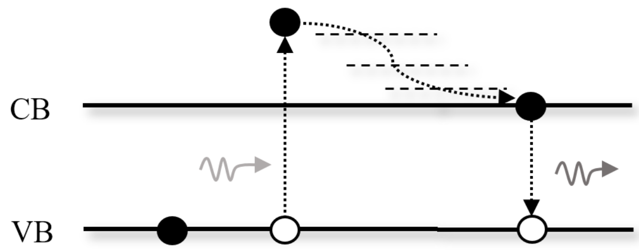

Fig. 1.4. Representation of the photoluminescence process. Adapted from [38].

For GaAsBi QWs, room-temperature (RT) PL analysis can be used to estimate the Bi content in the structure, taking into account the QW width and the Bi-induced bandgap reduction [36]. Here the incorporation of 1 % of Bi into GaAs lattice results in a lowering of the CB by ~ 28 meV and rising of the VB by ~ 30 – 65 meV [3, 19, 39]. In the case of Bi QDs, the RTPL peak wavelength can be studied for QD size approximation [15].

Temperature-dependent PL (TDPL) measurements allow to evaluate changes in the intensity of PL signal and the position of PL peak driven by temperature variations of the sample [37]. For example, the emission from GaAsBi QWs often display red-blue-red shift (S-shape) as a function of temperature, which is related to the carrier localization in potential fluctuations [9, 36]. This S-shape is attributed to the temperature-dependent redistribution of carriers between the localized states [40]. Excitation-dependent PL measurements are also useful, since they provide deeper insight into the dominant carrier recombination mechanisms (Fig. 1.5). At low temperature, PL intensity usually follows a linear dependence on excitation power, indicating radiative band-to-band recombination, whereas at RT a stronger power dependence is commonly observed due to the increased influence of non-radiative recombination processes [36, 40].

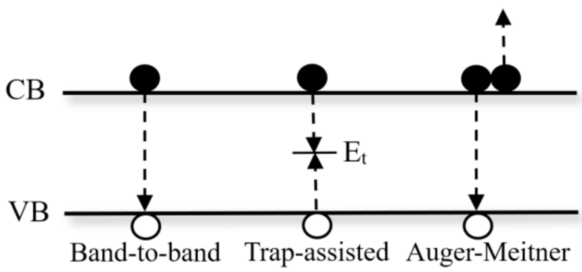

Fig. 1.5. Main carrier recombination mechanisms. Adapted from [41].

However, PL technique alone is not always sufficient for a complete optical study of bismide structures. For example, PL from a low density of emitting QDs may be too weak to detect. In such cases, cathodoluminescence (CL) can be useful complementary technique [17].

2 Experimental methodology

This section describes the equipment and devices used in the growth and characterization of the investigated structures. GaAsBi/AlGaAs parabolic quantum well structures were grown by molecular beam epitaxy method. Structural analysis was performed with high-resolution transmission electron microscopy (TEM) measurements, while optical investigation was conducted using cathodoluminescence and photoluminescence measurements.

2.1 Sample growth

Investigated samples were grown using the MBE method with Veeco GENxplor R&D MBE system. Epitaxial layers were deposited on semi-insulating GaAs substrates (350 µm), which were buffered by a GaAs layer. This study investigated different PQW structures, where rectangular GaAsBi QWs were embedded between 30 nm thick parabolically graded AlGaAs barriers. They were achieved by parabolically changing the Al content from 30% at the top of the barrier to 0% at the bottom. These quantum structures were sandwiched between AlGaAs layers and capped with a GaAs layer to prevent oxidation of the Al-containing alloy.

For the first set of samples, different growth and annealing conditions were used to study how distinct temperature regimes influence optical properties of GaAsBi QWs. Here the structural design of samples was kept as simple as possible with only one 6.8 nm GaAsBi QW (Fig. 2.1a). The distinguishing feature between the structures was the growth temperature used for the layers grown on top of GaAsBi QW (Fig. 2.1b). In the HT structure, these upper layers were grown at 650 °C, whereas in the LT structure, the temperature was kept at 455 °C. After the growth, each structure was cleaved into four pieces. One piece was kept as reference, while the remaining three were annealed in an RTA furnace at 650 °C, 700 °C and 750 °C for 180 s. As a result, a total of 8 samples were prepared for the first study presented in Section 3.1.

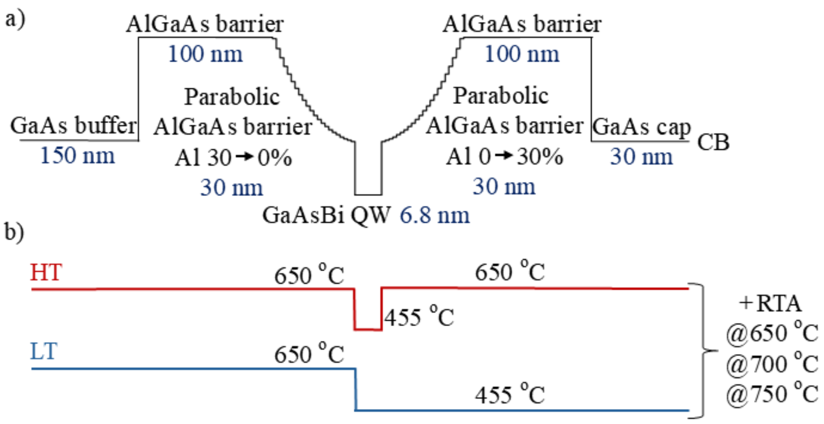

Fig. 2.1. a) Scheme and b) used growth temperatures of the investigated structures for the set 1.

The second part of this study (Section 3.2) is dedicated to one sample, which demonstrates how Bi clustering influences structural and optical properties of bismides. This sample contained two 7.3 nm GaAsBi PQWs separated by 30 nm thick AlGaAs layer (Fig. 2.2a). Structure was *in-situ* annealed at 730 °C for 144 s (Fig. 2.2b), which led to Bi QD formation. Additionally, piece of the sample was later *ex-situ* annealed at 700 °C for 180 s.

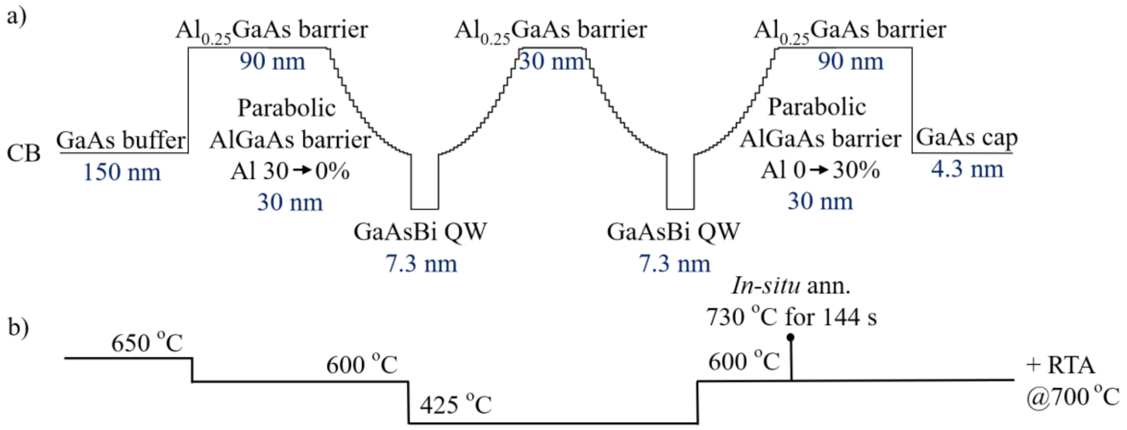

Fig. 2.2. a) Scheme and b) used growth temperatures of the investigated structures for set 2.

The final set of 4 samples were used to study how the introduction of ultrathin AlAs barriers affect the emission and structural properties of GaAsBi QW structures (Section 3.3). Here samples had two 14.5 nm rectangular GaAsBi QWs embedded between ultrathin AlAs and/or parabolically graded AlGaAs barriers (Fig. 2.3a). Samples were grown under the same temperature conditions, which are shown in Fig. 2.3b, however half of the samples were *in-situ* annealed at 750 °C for 110 s. The investigated samples differed by the presence and/or thickness of AlAs barriers (grown for 15 s or 10 s), as well as whether the *in-situ* annealing was performed.
Main information about all three sets of samples is presented in Table 2.1.

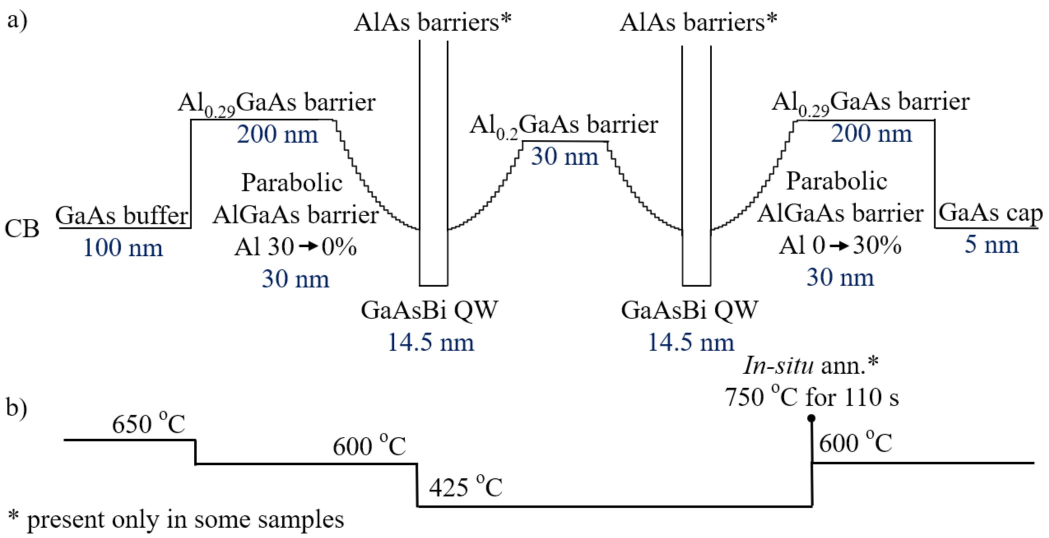

Fig. 2.3. a) Scheme and b) used growth temperatures of the investigated structures for set 3.

Table 2.1. Summary of sample sets used in the study.

Set	Investigated structures	Number of samples	Names of the samples
1	Single GaAsBi PQW with/without *in-situ* and *ex-situ* annealing	$2 + 3 \times 2$	HT; RTA@650 °C, RTA@700 °C, RTA@750 °C; LT; RTA@650 °C, RTA@700 °C, RTA@750 °C.
2	Double GaAsBi PQWs with/without *ex-situ* annealing	$1 + 1$	DWELL, RTA@700 °C.
3	Double GaAsBi PQWs with/without AlAs barriers and *in-situ* annealing	4	NoAlAs-NoAnn; AlAs-NoAnn; AlAs-Ann; ThinAlAs-Ann.

2.2 Transmission electron microscopy

Structural characterization was carried out using high-angle annular dark-field (HAADF) TEM on a FEI Tecnai G2 F20 X-TWIN TEM operated at 200 kV in scanning mode. The microscope was equipped with a Fischione 3000 HAADF detector for *Z*-contrast imaging and an energy-dispersive X-ray (EDX) detector for elemental mapping. Sample lamellas were prepared in an FEI Helios Nanolab 650 dual-beam system using an Omniprobe manipulator and were thinned by focused Ga^+ ion milling.

HAADF scanning transmission electron microscopy (STEM) micrographs were used to evaluate the overall structural quality of samples, including layer width uniformity and interface sharpness, as well as the presence of Bi QDs. Intensity profiles extracted from the STEM images were further employed to determine layer thicknesses and to assess the homogeneity of Bi incorporation within the GaAsBi QWs.

EDX measurements provided elemental analysis, allowing identification of the elements present and their distribution. This verified the formation of the Bi QDs within the GaAsBi QWs.

2.3 Cathodoluminescence measurements

CL measurements were performed with the sample mounted on a liquid helium cryostage inside a Zeiss Ultra55 SEM, which served as the electron source delivering high-energy electrons to excite the sample. The cryostage maintained a stable temperature of 10 K during the measurements. The CL signal was collected by a parabolic mirror and directed to the Horiba H-CLUE detection system. The electron beam was fixed at a single sub-nanometer spot and the emitted light intensity was recorded as a function of energy. This approach was used to probe luminescence from sparsely distributed Bi

QDs. Measurements were carried out at the Institute of Physics of the Polish Academy of Sciences in Warsaw.

2.4 Photoluminescence measurements

The photoluminescence measurement setup is presented in Fig. 2.4. For the temperature-dependent measurements, GaAsBi structures were mounted to the cold finger with thermal paste in a closed-cycle He cryostat. This setup, combined with a cryogenic temperature controller, enabled PL measurements across a wide temperature range from 4 K to 300 K. For RTPL measurements, the sample was positioned on a holder at the same position as in TDPL setup, after removing the cryostat from the optical path.

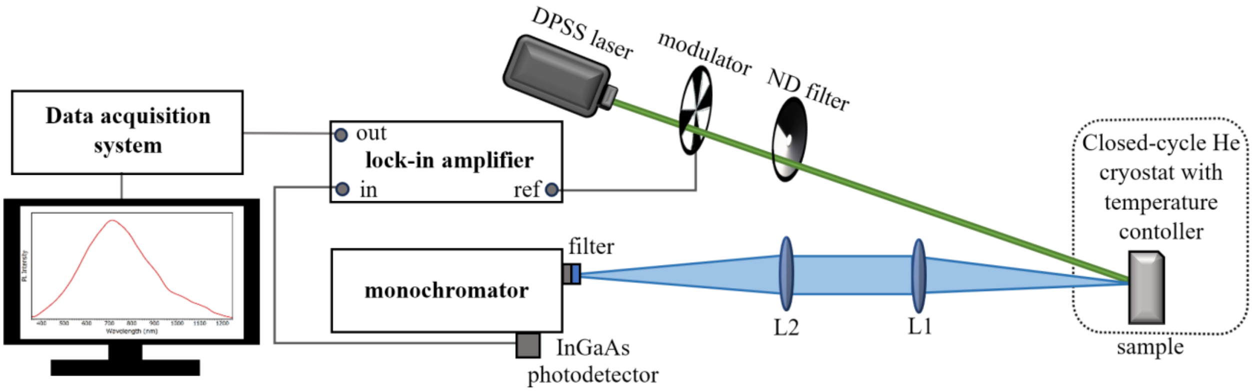

Fig. 2.4. Measurement scheme used for RTPL and TDPL.

Photoluminescence excitation was provided by a diode-pumped solid-state (DPSS) laser operating at a central wavelength of 532 nm with a maximum output power of 400 mW. The laser beam was modulated by an optical chopper wheel at 193 Hz , while excitation power was varied from 0.5 mW to 350 mW using radial gradient neutral density filter. The luminescence emitted from the sample was collected using a collimating L1 (f = 150 mm) and focusing L2 (f = 325 mm) lenses, before entering the monochromator (f = 500 mm). A cutoff filter was placed in front of the monochromator entrance slit to eliminate higher-order diffraction and laser radiation reflected from the sample. The signal detected by InGaAs photodetector was amplified using a synchronous lock-in amplifier, digitized by a data acquisition system and displayed on a computer screen.

The recorded PL spectra were then spectrally corrected to restore the original spectrum. This was achieved by dividing the measured signal by spectral response of the system and the correction curve obtained using a 100 W quartz halogen lamp. Finally, it was replotted as a function of photon energy $I_{PL}(\hbar\omega)$ [42].

For each sample series, all measurements were performed under the identical conditions using the same excitation powers to enable direct comparison of the PL spectra.

3 Results

This section presents results from structural measurements and analysis of optical properties of GaAsBi/AlGaAs PQW structures. Section 3.1 is dedicated to studying effects of *in-situ* and *ex-situ* annealing. Section 3.2 presents emission properties of Bi QDs, which have formed during thermal treatments. In section 3.3 structures with and without AlAs barriers and *in-situ* annealing are compared.

3.1 Annealing treatments

This study was carried out to assess the impact of annealing and identify the most effective thermal treatment process for enhancing emission properties of GaAsBi PQW structures. Samples were grown under two different MBE temperature protocols, employing low-temperature (LT sample) and high-temperature (HT sample) growths. In the latter case, the elevated growth temperature acted as unintentional *in-situ* annealing. Additionally, samples were *ex-situ* annealed at temperatures ranging from 650 °C to 750 °C. Structural analysis was performed using a STEM (see Section 3.1.1). The photoluminescence technique was employed to research the influence of thermal treatments on the optical quality of GaAsBi QWs (Section 3.1.2), which was reflected in emission intensity, thermal stability, carrier recombination and localization effects. The main results presented in this section were published in [14].

3.1.1 Structural changes

HAADF STEM images (Fig. 3.1) were used to evaluate compositional contrast and structural quality across the sample. Because HAADF STEM contrast scales with atomic number, where heavier elements appear brighter than lighter elements, GaAsBi QWs are visible as bright lines, grey zones correspond to AlGaAs barriers, while parabolically graded AlGaAs barriers are visible as a smooth intensity gradient. All presented layers look uniform in width and composition with sharp interfaces.

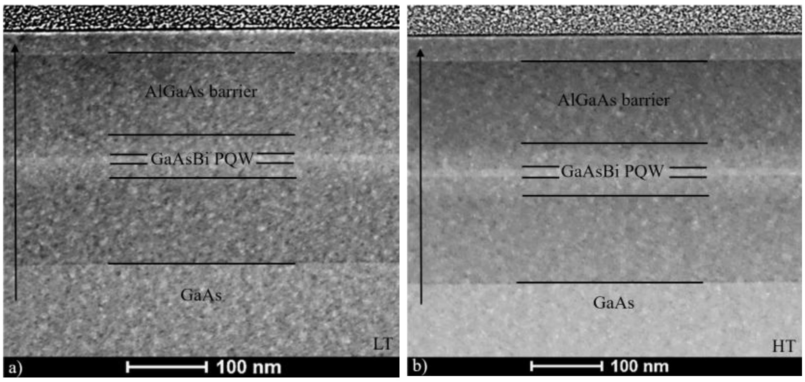

Fig. 3.1. HAADF STEM micrographs of: a) LT and b) HT GaAsBi/AlGaAs PQW structures. Black arrows represent the growth direction. Adapted from [14].

Fig. 3.2 and Fig. 3.3 show intensity profiles from the acquired STEM images. Here the central peak in each profile corresponds to the GaAsBi QW, while the lower intensity regions are attributed to AlGaAs barriers. The comparison of LT and HT structures shows very similar interface abruptness and layer dimensions, with estimated thicknesses of ~ 98 nm for the AlGaAs barriers, ~ 29 nm for the graded AlGaAs barriers and ~ 8 – 8.5 nm for the GaAsBi quantum wells.

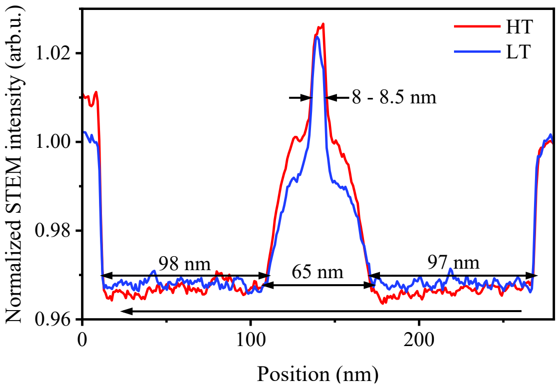

Fig. 3.2. Normalized intensity profiles of HAADF STEM images after background subtraction. Black arrow represents the growth direction. Taken from [14].

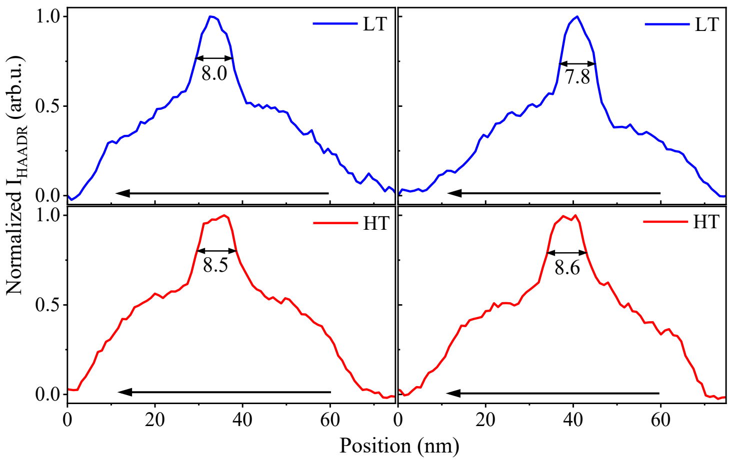

Fig. 3.3. Enlarged sections of the HAADF STEM intensity profiles of LT and HT GaAsBi/AlGaAs PQW structures at two different areas on each sample. Black arrows represent the growth direction. Taken from [14].

Fig. 3.3 shows enlarged sections of the HAADF STEM intensity profiles taken across the PQW region at two different areas on each sample. The LT sample exhibits slightly narrower QW peaks, consistent with suppressed Bi diffusion during low-temperature growth. By contrast, the HT sample shows broader QW peaks, indicative of enhanced Bi mobility at elevated temperatures, however, the presence of Al in the barriers appears to limit Bi diffusion and constrain the overall well thickness, so the HT wells are comparatively more uniform in width. Moreover, the profiles of HT sample appear flatter across the QW top, suggesting a more homogeneous Bi composition, whereas the LT profiles show a sharper central maximum consistent with a more localized Bi concentration. Lastly, the parabolically graded AlGaAs barrier profiles in the LT sample have slightly less symmetry, which is attributed to different substrate temperatures used during their growth.

Overall, TEM revealed that employed high-temperature growth does not compromise the QW structural quality and improves the homogeneity of Bi concentration in it.

3.1.2 Optical properties

GaAsBi crystal quality is strongly influenced by the growth temperature, thus, it was expected that *in-situ* and *ex-situ* annealing will have a pronounced effect on emission of investigated structures, therefore RTPL, excitation-dependent PL and TDPL measurements were performed.

3.1.2.1 Room-temperature photoluminescence

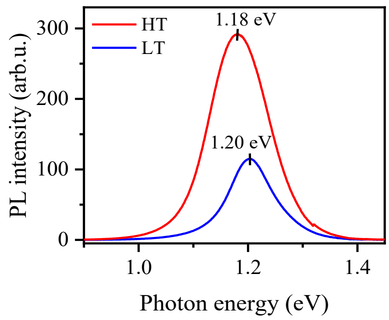

Fig. 3.4. RTPL spectra of investigated GaAsBi/AlGaAs PQW structures. Taken from [14].

Figure 3.4 presents the RTPL spectra. PQW structures exhibit one PL band of 1.18 eV (HT) and 1.20 eV (LT), which is attributed to the optical transition in GaAsBi QW with ~ 4 – 4.5 %Bi. Here Bi content is obtained by fitting the measured RTPL spectra to the calculated optical transition energies [36]. PL peak position of HT structure exhibits a small red-shift, which can be explained by the increased Bi concentration or broadening of the QW width due to enhanced bismuth diffusion during the elevated-temperature growth phases [30].

It can be seen that the *in-situ* annealing also resulted in the increase of RTPL peak intensity, where HT structure exhibits higher PL intensity than structure grown at low-temperature. This PL intensity gain can be explained by the reduction of point defects via high-temperature growth phase, which led to the self-annealing of the HT structure during the MBE growth. Here, the content of non-radiative recombination centers, like interface defects [43] or Bi pair defects [32], gets reduced as the high-temperature regime is applied. As a result, high-temperature growth regime was found to be preferable for enhancing RTPL intensity.

To get deeper understanding into *in-situ* annealing impact on carrier recombination mechanisms, PL intensity dependence on excitation power (Fig. 3.5) was measured and fitted with power law (eq. 1) [44]. Here extracted slope m provides information about the dominant recombination mechanism, where $m \approx 1$ corresponds to radiative (band-to-band) recombination, $m \approx 2$ to Shockley-Read-Hall (trap-assisted) non-radiative recombination and $m \approx 2/3$ to Auger recombination [40].

$$I_{\mathrm{PL}} \propto P^{m}, \tag{1}$$

here m denotes the recombination process.

1.40 and 1.53 slope values for HT and LT structures were evaluated. This confirms that high-temperature growth regime reduces non-radiative recombination processes.

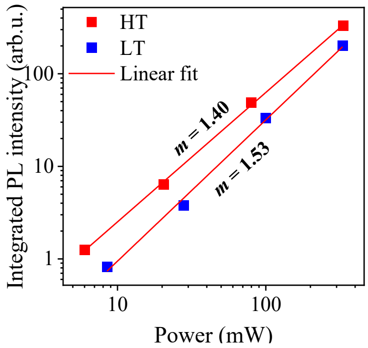

Fig. 3.5. Integrated RTPL intensity dependence on excitation power. Dependencies are fitted with power law (eq. 1). Adapted from [14].

To investigate the effect of *ex-situ* post-growth annealing, each sample was initially measured before and then after RTA. These RTPL spectra are presented in Fig. 3.6 and Fig. 3.7 for HT and LT structures, respectively. Here samples were excited with excitation power of ~ 80 mW. Moreover, each presented RTPL spectra displays quantitative value of positive or negative impact on PL intensity after thermal annealing.

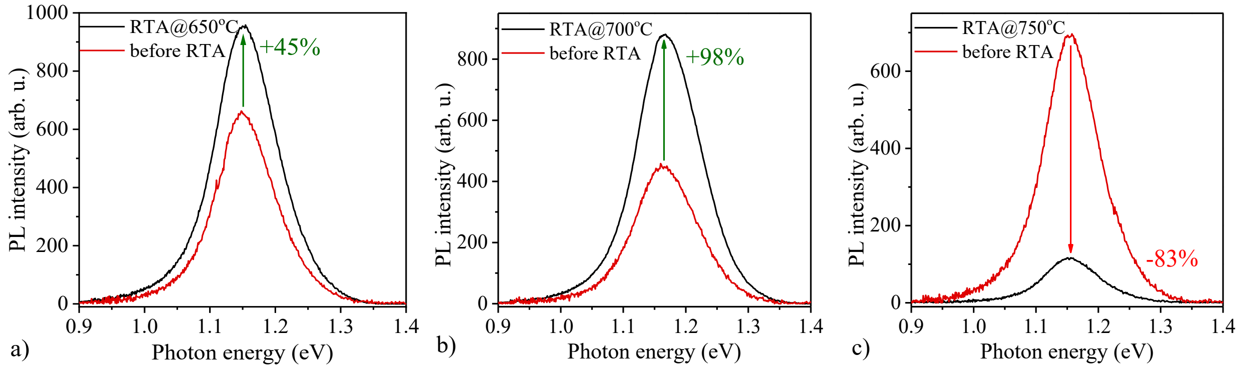

Fig. 3.6. RTPL spectra of GaAsBi/AlGaAs PQW HT structures before and after rapid thermal annealing at: a) 650 ºC, b) 700 ºC and c) 750 ºC. Taken from [14].

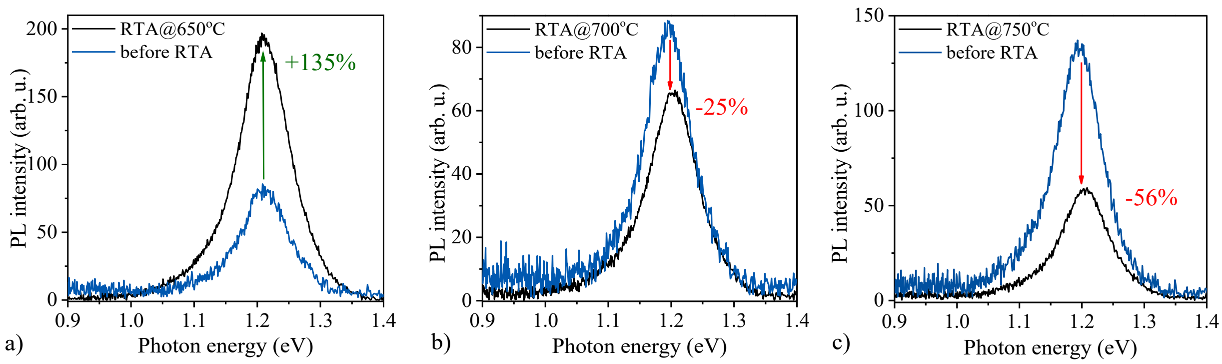

Fig. 3.7. RTPL spectra of GaAsBi/AlGaAs PQW LT structures before and after rapid thermal annealing at: a) 650 ºC, b) 700 ºC and c) 750 ºC. Taken from [14].

In HT structure post-growth annealing at 650 ºC and 700 ºC resulted in increased RTPL intensities, while RTA at 750 ºC caused degradation of the PL signal, which could be associated with the worsening of the structural quality [45] or activation of additional non-radiative centers [46]. LT structure started showing a decrease in RTPL intensity at lower annealing temperatures, and here the increase in intensity can be seen only after RTA at 650 ºC. This PL intensity gain can be explained by the expected reduction of defects in GaAsBi QW layer [10, 11], which reduced the non-radiative recombination centers.

It can be observed, that applied *in-situ* annealing affected the thermal stability of the PQW structures, where HT sample could benefit from higher RTA temperatures (up to 700 ºC) before the signs of degradation appeared. Higher than optimal RTA temperatures decreased RTPL peak intensities due to the over-annealing resulting from the Bi segregation, cluster formation [17, 18], interface interdiffusion or formation of non-radiative recombination centers [45, 46].

It should be mentioned that all samples exhibited a small blue-shift of the PL peak position after RTA, which can be explained by the reduction of Bi concentration in GaAsBi QWs due to diffusion, clustering or segregation.

All in all, room-temperature PL measurements revealed that high-temperature growth resulted in unintentional *in-situ* annealing of the PQW structure: increased emission intensity (Fig. 3.4), reduced non-radiative recombination processes (Fig. 3.5) and improved thermal stability (Fig. 3.6, Fig. 3.7), which was evaluated from the stability of the PL peak intensity after post-growth RTA treatments. *Ex-situ* annealing also played a significant role in emission of PQW structures: it blue-shifted the PL peak position and changed the RTPL intensity. The increase or decrease in the emission intensity depended on the applied RTA temperature.

3.1.2.2 Temperature-dependent photoluminescence

TDPL measurements were carried out in the 4 – 300 K temperature range under the ~ 20 mW excitation. Measured spectra (Fig. 3.8) showed PL band position and intensity dependence on temperature variations. Firstly, it can be observed that structures display red-blue-red bandgap shift when temperatures were increased, which shows that there is carrier localization in the investigated samples [40]. The presence of the localization effect is typical in GaAsBi structures and it suggests that Bi is distributed inhomogeneously in GaAsBi QWs, creating potential fluctuations. The low temperature red-blue shift corresponds to carrier redistribution between deep and shallow localized states, while the red-shift at higher temperatures results from the typical semiconductor bandgap narrowing. The bandgap reduction and carrier localization can be quantified by fitting the temperature dependence of the PL peak energy with the Varshni-Eliseev function [47]:

$$E_g = E_0 - \frac{\alpha T^2}{\beta + T} - \frac{\sigma^2}{k_B T}, \quad (2)$$

where, E_g is the bandgap energy [eV], E_0 is the bandgap energy at 0 K temperature [eV]. Varshni parameter α shows the bandgap shift per unit temperature [meV/K], while parameter β is related to the Debye temperature [K]. Meanwhile. the Eliseev parameter σ describes the dispersion among localized states assuming a Gaussian distribution [meV].

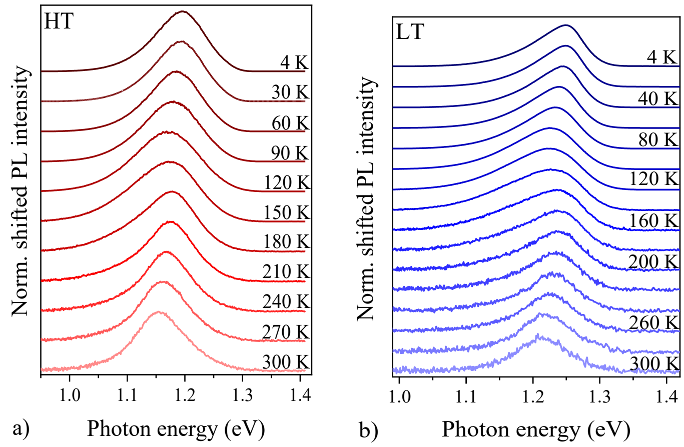

Fig. 3.8. TDPL spectra of: a) HT and b) LT structures under 20 mW excitation. Taken from [14].

Therefore, the experimental data was fitted using Varshni-Eliseev function (eq. 2), as presented in Fig 3.9a. Acquired data (Table 3.1), specifically the Eliseev parameter σ, shows localization effect.

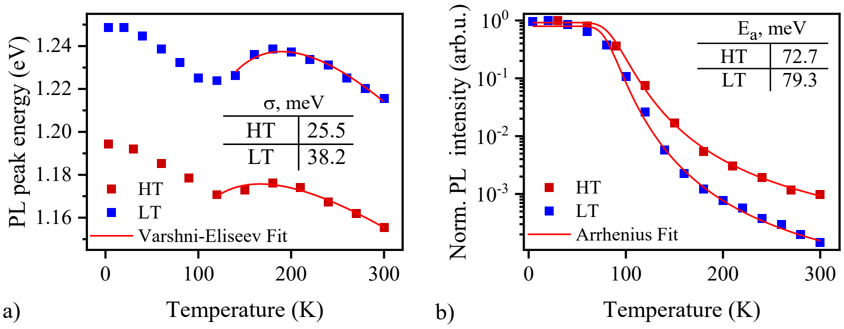

Fig. 3.9. TDPL measurements: a) PL peak position dependence on the temperature fitted with Varshni-Eliseev function [47] (eq. 2), b) PL intensity dependence on the temperature fitted with Arrhenius-type expression [40] (eq. 3). Taken from [14].

Table 3.1. Obtained fitting parameters from TDPL measurements of Varshni-Eliseev function (eq. 2). Taken from [14].

Structure	E_0 , eV	α, meV/K	β (fixed)[48], K	σ, meV
HT	1.25	0.39	204	26
LT	1.38	0.64		38

Stronger localization was observed in LT structure (38 meV). Lower carrier localization effect in HT sample of 26 meV was attributed to the high-temperature growth regime, having more uniform Bi distribution in GaAsBi QW. As the estimated localization energies are higher than the thermal energy at room temperature, carriers are expected to be localized even at RT in both PQW structures.

To analyse thermal PL quenching, integrated PL intensity was plotted as a function of temperature in Fig. 3.9b. Experimental data was fitted using Arrhenius equation [40]:

$$I(T) = \frac{I_0}{1 + \sum_n \alpha_n \, exp\left(-\frac{E_{a_n}}{k_B T}\right)}, \tag{3}$$

where I_0 is the PL intensity at 0 K and α_n is fitting coefficient related to the activation energy E_{a_n} with n indexing different recombination channels.

It can be seen that thermal PL intensity quenching decreased for HT structure, which can be explained by the improved crystal quality during unintentional *in-situ* annealing.

Acquired activation energy E_a (73 meV (HT) and 79 meV (LT)) was attributed to the thermal delocalization of carriers [40]. Here higher activation energy for the LT structure coincided with larger carrier localization as depicted in Fig. 3.9a, while *in-situ* annealed structure exhibited lower activation energy and therefore shallower traps.

TDPL measurements revealed that *in-situ* annealed structure exhibited lower carrier localization, reduced bandgap sensitivity to temperature and weaker PL intensity quenching, which was attributed to improved structural quality of the sample.

All in all, this study showed that *in-situ* annealing can enhance structural and optical properties of PQW structures: improving Bi compositional uniformity, increasing emission intensities and allowing structures to tolerate and benefit from higher *ex-situ* annealing temperatures.

3.2 Dot-in-a-well structure

Thermal treatment can also promote unwanted Bi migration and segregation in GaAsBi quantum structures. As discussed in this section, such Bi redistribution leads to clustering and formation of Bi QDs, while simultaneously distorting the QW structure through degradation of its heterointerfaces. This can be observed in Fig. 3.10, where HAADF STEM micrographs of investigated GaAsBi PQW (DWELL) sample reveal disordered structure with Bi QDs of varying size (visible as bright spots in Fig. 3.10a and dark circles in Fig. 3.10b), inhomogeneous GaAsBi QWs and blurred interfaces. This indicate that applied growth conditions (high-temperature growth of subsequent barriers after QW deposition, together with additionally applied *in-situ* annealing) promoted interlayer Bi diffusion.

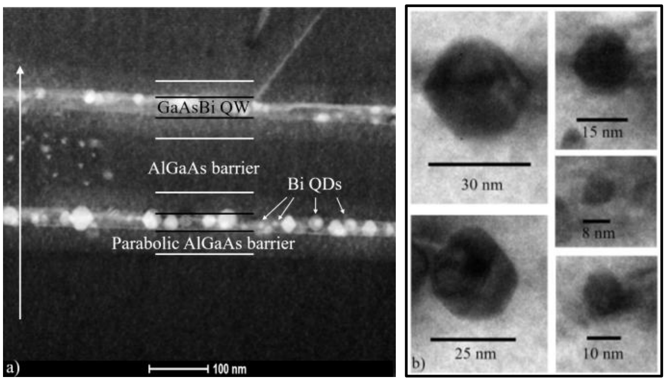

Fig. 3.10. HAADF STEM micrographs of: a) DWELL sample and b) enlarged sections of Bi QDs with varying sizes. White arrow represents the growth direction.

3.2.1 Emission properties

Although the investigated DWELL sample exhibited visible disorder of the heterostructure (Fig. 3.10) and was not expected to have emission from such degraded GaAsBi QWs, strong luminescence was still observed in the PL spectra (Fig. 3.11). For more detailed analysis of the observed emission, this DWELL sample was additionally *ex-situ* annealed at 700 ºC. RTPL measurements revealed no significant changes in emission energy or spectral shape after annealing (Fig. 3.11). Therefore, considering the degraded QWs observed by TEM and the presence of QDs in the structure, the detected PL emission was presumed to originate from the Bi QDs. Furthermore, based on the reported dependence of the Bi QD bandgap on its size [15], the broad RTPL band observed at ~ 1.1 eV would correspond to Bi QDs with a diameter of ~ 6 – 9 nm.

Carrier recombination mechanisms were evaluated by fitting LTPL and RTPL intensity dependences on excitation power using power law (eq. 1) (Fig. 3.12). The extracted slope parameter *m* was found to be ~ 1.0 at 4 K and increased to ~ 1.3 – 1.6 at RT. This indicates dominant radiative recombination at low temperatures and an increasing contribution of non-radiative recombination processes at higher temperatures.

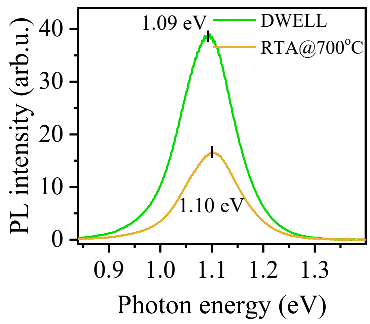

Fig. 3.11. RTPL spectra of investigated DWELL structure before and after RTA.

The reduced *m* value after *ex-situ* annealing at 700 ºC may indicate reduction of non-radiative recombination centers in the surrounding QD region of the sample. However, the simultaneous decrease in PL intensity (Fig. 3.11 and Fig. 3.12) suggests that RTA redistributes Bi between existing QDs, modifying their size distribution and emissive efficiency, where smaller emissive QDs may merge into larger Bi-rich clusters exhibiting weaker carrier confinement and therefore poorer optical properties.

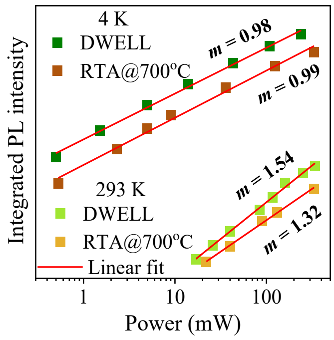

Fig. 3.12. Integrated LTPL and RTPL intensity dependences on excitation power. Dependencies are fitted with power law (eq. 1).

To further analyse the emission properties of the DWELL structure, TDPL measurements were carried out at 4 – 300 K under 50 mW excitation (Fig. 3.13). Visible redistribution of the spectral shape at low temperatures (4 – 50 K) is due to enhanced emission on the low-energy side of the PL band after RTA, which also suggest possible formation of larger QDs through merging of smaller ones.

To better visualize and investigate the changes in the emission position, the PL peak position dependence on temperature was plotted in Fig. 3.14a and fitted using the Varshni-Eliseev function (Table 3.2). TDPL measurements showed strong carrier localization of 21 meV (DWELL) and 34 meV (RTA@700°C). This localization effect can be explained by the carrier thermalization and recapture processes [49, 50]. The low-temperature red-blue shift corresponds to carrier redistribution among closely spaced Bi QDs with non-uniform size distribution, where PL emission shift arises from different size of QDs [34, 35, 51]. At higher temperatures, the observed redshift is associated with the typical semiconductor bandgap narrowing.

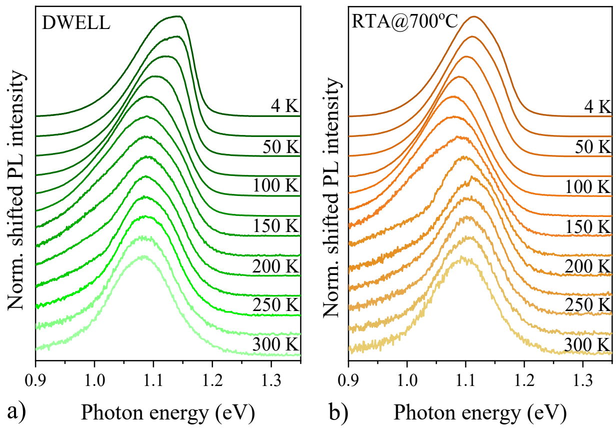

Fig. 3.13. TDPL spectra of: a) DWELL and b) RTA@700°C structures under 50 mW excitation.

Moreover, the increased carrier localization observed after *ex-situ* annealing is consistent with modified size distribution of QDs caused Bi redistribution during RTA. Here formation of larger Bi QDs provides lower-energy states and therefore dominates the low-temperature (4 – 100 K) emission, resulting in a red-shifted PL peak. The enhanced blue-shift at intermediate temperatures (100 – 200 K) indicates broader distribution of localized states, while bandgap shrinkage at high temperatures (200 – 300 K) leads to a typical red-shift of PL peak.

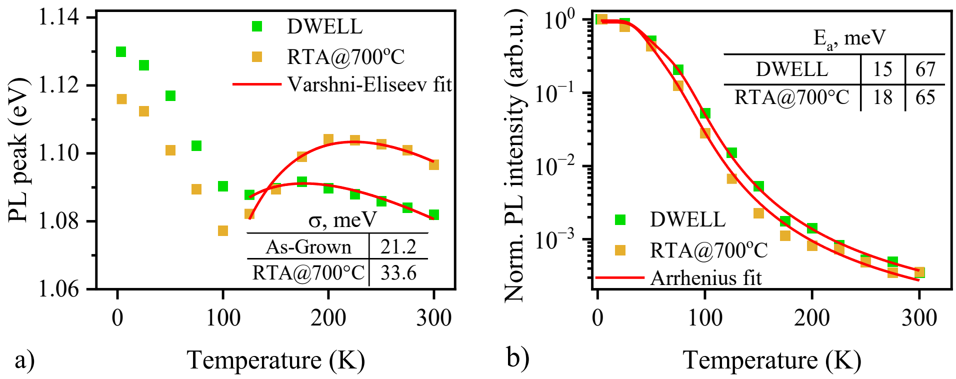

Fig. 3.14. TDPL measurements of DWELL and RTA@700°C samples: a) PL peak position dependence on the temperature fitted with Varshni-Eliseev function [47] (eq. 2), b) PL intensity dependence on the temperature fitted with Arrhenius-type expression [40] (eq. 3).

Table 3.2. Obtained fitting parameters from TDPL measurements with Varshni-Eliseev function (eq. 2).

Structure	E_0 , eV	α, meV/K	β (fixed)[48], K	σ, meV
DWELL	1.14	0.24	204	21
RTA@700°C	1.20	0.34		34

TDPL intensity quenching was analysed (Fig. 3.14b) and fitted with a modified Arrhenius equation (eq. 3) with two thermal activation energies, E_{a1} and E_{a2}. The obtained thermal quenching behaviour is very similar for both samples. Consistent with the excitation power-dependent measurements, this indicates that RTA does not significantly alter the dominant carrier recombination mechanisms and the origin of the emission remains unchanged.

Additionally, TDPL measurements for the DWELL sample were carried out using different excitation powers of 5 mW, 50 mW and 350 mW (Fig. 3.15). It was observed that the PL peak exhibited a blue-shift at low temperatures and reduced carrier localization with increasing excitation density (see Fig. 3.15a and Table 3.3). This can be explained by the state-filling effect, where the lowest-energy localized states become progressively occupied as the excitation power increases, so additional carriers recombine from higher-energy states [52]. This effect also accounts for slower thermal PL quenching and the decrease in acquired activation energies with increasing excitation power (Fig. 3.15b), as the occupation of the lowest energy states results in emission from shallower confinement states [53]. The extracted activation energies of 10 – 20 meV and 60 – 75 meV can be assigned to thermal redistribution among shallow localized states and to carrier escape from QDs into the surrounding non-radiative recombination centers, respectively [54].

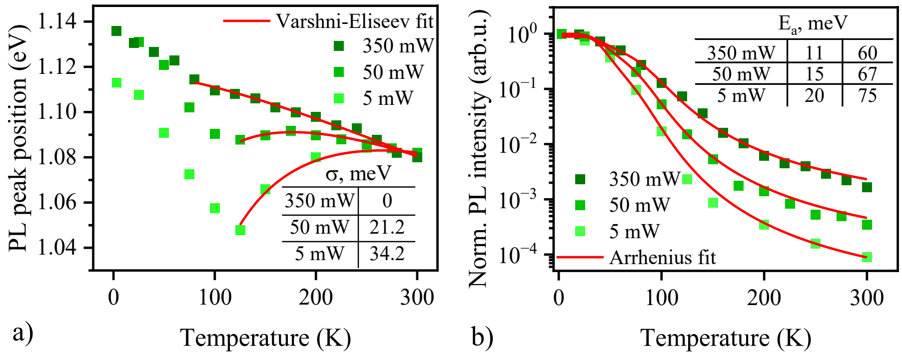

Fig. 3.15. TDPL measurements under different excitation powers: a) PL peak position dependence on the temperature fitted with Varshni-Eliseev function [47] (eq. 2), b) PL intensity dependence on the temperature fitted with Arrhenius-type expression [40] (eq. 3).

Table 3.3. Obtained fitting parameters from TDPL measurements with Varshni-Eliseev function (eq. 2).

Excitation power, mW	E_0 , eV	α, meV/K	β (fixed)[48], K	σ, meV
350	1.12	0.21		0
50	1.14	0.23	204	21
5	1.17	0.24		34

All in all, it was shown that annealing-induced Bi redistribution in GaAsBi PQWs can result in the formation of emissive Bi QDs, whose optical properties were analysed. However, this process also leads to degradation of the heterostructure due to Bi migration and segregation, while formed QDs exhibit a wide and poorly controlled size distribution. This behaviour is attributed to the insufficient suppression of Bi diffusion in PQW structures, where the region adjacent to the QW consists of GaAs and AlGaAs barriers with low Al content, highlighting the need for additional methods enabling controlled QD formation without structural degradation.

3.3 Structures with ultrathin AlAs barriers

A key advantage of Bi QD emission is that its wavelength can be tuned by controlling the dot size [15]. In section 3.3.1, this idea is realized by introducing additional AlAs barriers between the GaAsBi QW and the parabolic barriers. Furthermore, the effect of AlAs barriers on the emission from the GaAsBi QWs is also considered and analysed (see Section 3.3.2). Here four GaAsBi PQW structures were investigated, namely NoAlAs-NoAnn (reference sample without AlAs barriers), AlAs-NoAnn (sample with AlAs barriers), AlAs-Ann (sample with AlAs barriers and *in-situ* annealing) and ThinAlAs-Ann (sample with reduced AlAs barrier thickness and *in-situ* annealing).

3.3.1 Size control of Bi quantum dots

This part of the study focuses on a structure with AlAs barriers that underwent *in-situ* annealing (AlAs-Ann sample). The aim was to evaluate whether the AlAs barriers can control the size of Bi quantum dots while preventing degradation of the heterointerfaces.

The HAADF STEM micrographs (Fig. 3.16 and Fig. 3.19c) revealed two uniform QWs sandwiched between clearly defined AlAs barriers, as well as Bi clusters formed in the first QW. It can be seen that AlAs barriers effectively limited the Bi QD size within the QW and prevented degradation of the structural quality. Lower density of Bi QDs observed in this structure, compared to the DWELL sample, can be attributed to the lower growth temperature of the parabolic AlGaAs barrier after GaAsBi QW deposition, which prevented unintentional *in-situ* annealing of the uncovered GaAsBi layer. In addition, better structural quality of the AlAs-Ann sample, which does not further promote Bi diffusion [55, 56], can also contribute to the reduced QD formation.

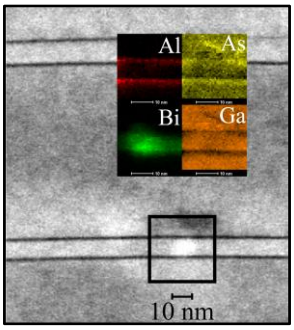

Fig. 3.16. HAADF STEM micrograph of a Bi QD in a GaAsBi PQW structure with AlAs barriers. The corresponding EDX maps show the elemental distribution of Al, As, Bi and Ga.

Fig. 3.16 shows the STEM image of a Bi QD in a GaAsBi QW together with EDX elemental maps of Al, As, Bi and Ga obtained from the selected region indicated in the image. The size of the observed Bi QD can be estimated to be comparable to the QW width.

Emission from this structure was recorded using CL (Fig. 3.17) and PL (Fig. 3.18) techniques. Low-temperature CL (LTCL) spectra exhibited two distinct emission bands. Here broad CL peak at ~ 1.15 eV was attributed to optical transitions in GaAsBi QW, while sharp band at ~ 0.93 eV was associated with emission from Bi QDs. Based on the emission energy and the dependence of the effective bandgap on QD dimensions (see Fig. 3.17 inset [15]), the QD size was estimated to be approximately 9 nm. The determined diameter shows good agreement with the QD dimensions observed in TEM images.

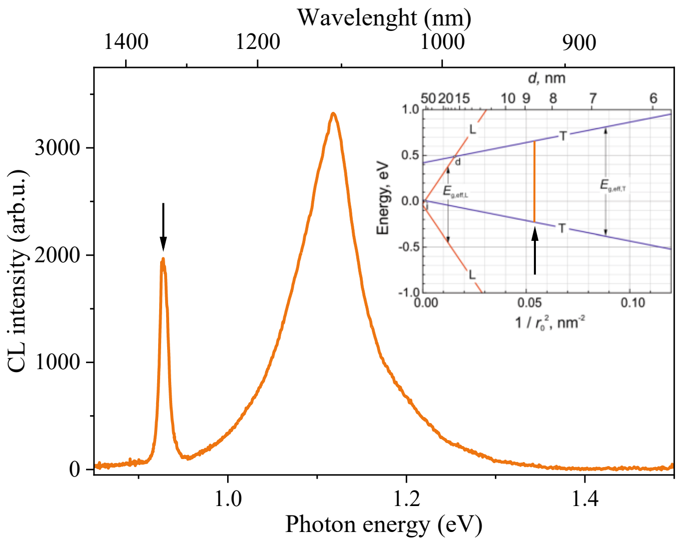

Fig. 3.17. LTCL spectra of investigated GaAsBi/AlGaAs PQW structure with Bi QDs (sample AlAs-Ann). CL peak at ~ 0.93 eV corresponds to emission from ~ 9 nm Bi QDs (calculated from inset [15]).

While emission from Bi QDs was observed in CL measurements, no corresponding PL emission band was detected in either RTPL (Fig. 3.18a), or LTPL (Fig. 3.18b) spectra. The absence of Bi QD PL emission is likely due to the low density of QDs and the dominance of recombination in the structurally intact GaAsBi QWs. In contrast, CL measurements enabled localized excitation, allowing emission from individual QDs to be detected.

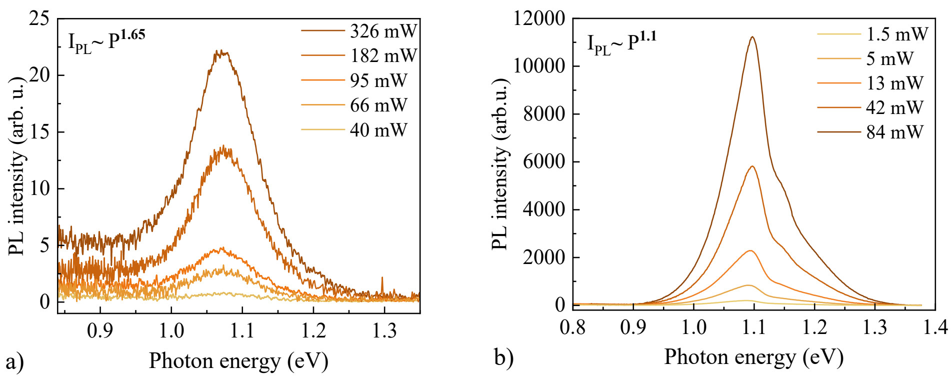

Fig. 3.18. a) RTPL and b) LTPL spectra using different excitation power of GaAsBi/AlGaAs PQW structure with Bi QDs (sample AlAs-Ann).

PL measurements were performed over a wide range of excitation powers from 40 mW to 326 mW at RT and from 1.5 mW to 84 mW at LT. Measured PL intensity dependence on excitation power was analysed using a power law fit (eq. 1), where slope parameter m was found to be 1.65 and 1.1 for RT and LT measurements, respectively.

3.3.2 Effect on GaAsBi quantum wells

Interestingly, it was noticed that, without the effect of controlling the size of Bi QDs, AlAs barriers also tend to affect structural and optical properties of GaAsBi QWs. Therefore, structures with and without AlAs barriers and annealing treatments were additionally investigated.

3.3.2.1 Structural analysis

Structural characterization employing HAADF STEM images and corresponding intensity profiles (Fig. 3.19) was used to evaluate compositional contrast and structural quality across the samples.

STEM micrographs showed that all structures have uniform thickness and composition layers with relatively sharp interfaces.

Introduced AlAs barriers can be observed in figure 3.19 b), c) and d) as dark lines in HAADF STEM images. It can be noticed that in AlAs-NoAnn and ThinAlAs-Ann samples AlAs barriers above QW layers either did not form or were significantly thinner than expected. This could be explained by Bi surface segregation, where Bi-rich growth front remaining after QW deposition alters Al incorporation, suppressing its nucleation and leading to incomplete or delayed AlAs growth, which produces an apparent reduction in average AlAs thickness.

It also should be noted that the observed slopes in the intensity profiles (Fig. 3.19, right) result from variations in lamella thickness and therefore should not be interpreted as a structural feature.

Comparing the structures revealed that the introduction of AlAs barriers yields more uniform GaAsBi QW widths (Fig. 3.19c, Fig. 3.19d). This effect was attributed to the AlAs layers acting as Bi-blocking barriers that suppressed Bi diffusion and/or segregation, thereby preventing broadening of the QWs [16].

Moreover, notable differences were observed between structures with and without thermal treatments, where samples without *in-situ* annealing showed more inhomogeneous Bi distribution within the wider GaAsBi QWs (Fig. 3.19a, Fig. 3.19b). This visible initial Bi-rich peak followed by a decrease in Bi concentration was attributed to the growth procedure, where a growth interruption is made before QW deposition to form a Bi wetting layer. This is traditionally used to prevent the delayed incorporation of Bi into the GaAs lattice [57], however it can also lead to the observed compositional non-uniformity.

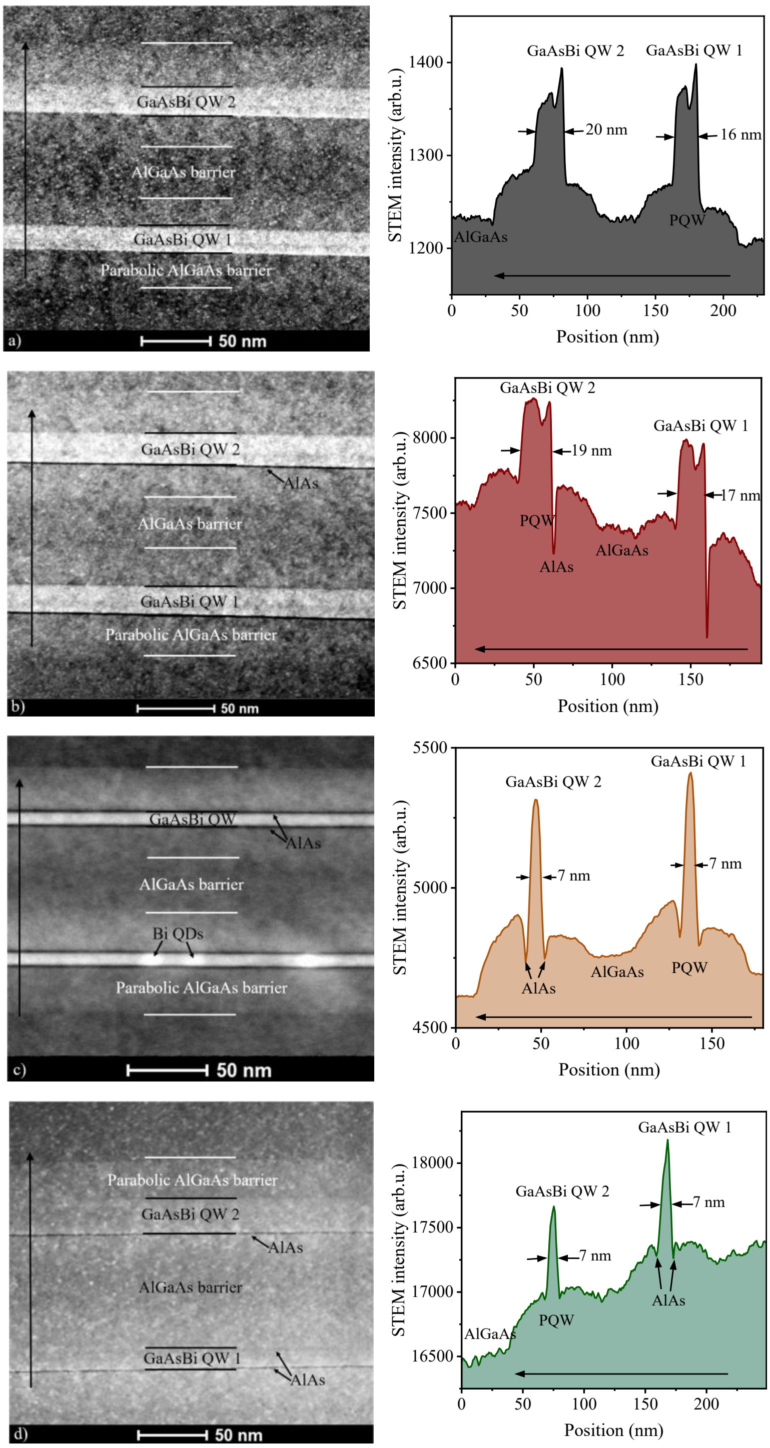

Fig. 3.19. HAADF STEM micrograph (left) and intensity profile (right) of: a) NoAlAs-NoAnn, b) AlAs-NoAnn, c) AlAs-Ann and d) ThinAlAs-Ann samples. Black lines represent growth directions.

3.3.2.2 Optical investigation

While the introduction of AlAs barriers resulted in improved structural uniformity of the samples, the optical quality of such QWs was found to be degraded. RTPL spectra of investigated structures is presented in Fig. 3.20. RTPL bands of 1.12 eV (NoAlAs-NoAnn), 1.07 eV (AlAs-NoAnn), 1.15 eV (AlAs-Ann) and 1.08 eV (ThinAlAs-Ann) were attributed to the optical transitions in 7 nm GaAsBi QWs with ~ 7 %Bi for *in-situ* annealed samples and 17 nm GaAsBi QWs with ~ 5 %Bi for samples without annealing treatments. Here Bi concentration was determined by matching the calculated optical transition energies to the experimental RTPL spectra [36], while accounting for the quantum well widths determined from TEM analysis. It can be observed that annealed samples exhibit higher Bi concentrations in thinner QWs. This can be attributed to enhanced Bi mobility and incorporation into the lattice during high-temperature treatments [30], combined with thermally driven Bi clustering into visible QDs and/or diffusion, which produced thinner and locally Bi-richer QWs.

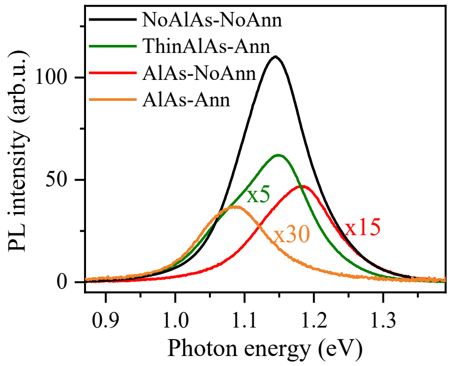

Fig. 3.20. RTPL spectra of investigated structures (AlAs-Ann, AlAs-NoAnn and ThinAlAs-Ann samples were multiplied for better visualization).

RTPL measurements (Fig. 3.20 and Fig. 3.21) showed that the highest PL intensity is obtained for the sample without AlAs barriers, while their introduction significantly reduces the optical response for both AlAs-NoAnn and AlAs-Ann samples, indicating that AlAs incorporation worsens optical performance of bismides. These observations can be explained by a non-optimal AlAs growth temperature, which promotes defect formation [58]. However, a noticeable increase in RTPL intensity can be observed for the ThinAlAs-Ann sample, where the AlAs barriers were grown thinner and structure was thermally treated, suggesting that the optical response of GaAsBi/AlGaAs PQWs depends not only on the presence of AlAs barriers.

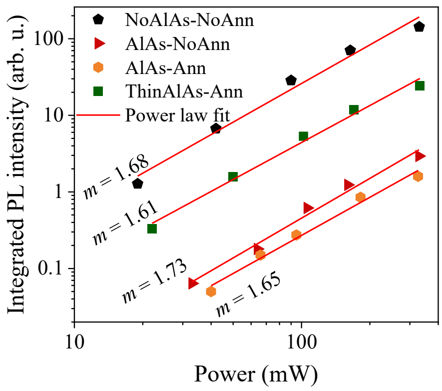

Fig. 3.21. Integrated RTPL intensity dependence on excitation power. Dependencies are fitted with power law (eq. 1).

This trend is further confirmed by RTPL intensity dependence on excitation power, which is shown in Fig. 3.21. Presented data was fitted using the power law (eq. 1), where obtained slope m values fall in the range of 1.61 – 1.73, suggesting that more than one mechanism is responsible for recombination. It can be observed that the addition of AlAs barriers correlates with an increase in m

value from 1.68 to 1.73, consistent with degraded optical behaviour. However, this slope parameter can be improved by thermal treatment to 1.65 and with thinning the AlAs barriers to 1.61, showing that growth and annealing modifications can improve the adverse optical effects introduced by AlAs. TDPL measurements were performed in the 4 – 300 K range using an excitation power of 73 mW (Fig. 3.22). Measured spectra showed a characteristic S-shaped temperature dependence of PL peak position (Fig. 3.23a). Therefore, the experimental data was fitted using Varshni-Eliseev function (eq. 2).

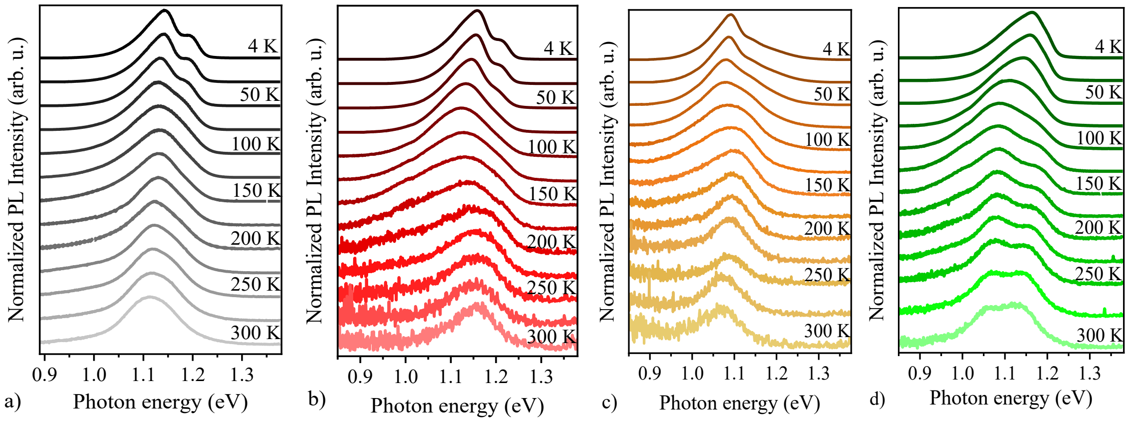

Fig. 3.22. TDPL spectra using an excitation power of 73 mW (normalized and shifted for better visualization of: a) NoAlAs-NoAnn, b) AlAs-NoAnn, c) AlAs-Ann and d) ThinAlAs-Ann samples.

Acquired data (Table 3.4) showed carrier localization effect ranging from 11 – 25 meV. Carrier localization was caused by potential fluctuations within GaAsBi QWs and/or blurred interfaces between layers. The data show a systematic increase in localization with the presence and thickness of AlAs barriers. Here NoAlAs-NoAnn structure had the lowest localization, which increased as thin AlAs barriers were formed in AlAs-NoAnn and ThinAlAs-Ann structures and was largest when both thick AlAs barriers were formed in AlAs-Ann structure.

Consistent with the localization results, thermal quenching of the PL (Fig. 3.23b) was the slowest for the sample without AlAs and increased for samples with AlAs barriers. The slowest PL intensity quenching in samples with AlAs barriers was visible in ThinAlAs-Ann sample, whereas structures with thicker AlAs barriers showed faster quenching. Additionally, thermal PL intensity quenching process was fitted using Arrhenius expression (eq. 3). Acquired activation energies E_{a1} (10 – 15 meV) and E_{a2} (60 – 80 meV) were attributed to thermal detrapping from shallow Bi-related localized states [36] and activation of non-radiative recombination channels associated with defects [40], respectively. The extracted activation energies E_{a2} follows the previously observed trend of degraded optical quality upon the introduction of AlAs barriers, with the lowest E_{a2} value observed for the NoAlAs-NoAnn structure and the highest for the AlAs-Ann sample. This behaviour was attributed to the creation of defects in the interfaces between AlAs and QWs or barriers [58].

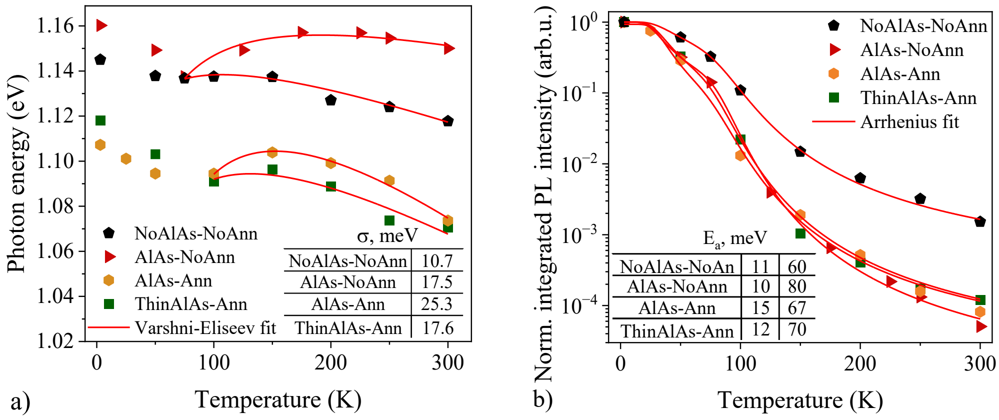

Fig. 3.23. TDPL measurements: a) PL peak position dependence on the temperature fitted with Varshni-Eliseev function [47] (eq. 2), PL intensity dependence on the temperature fitted with Arrhenius-type expression [40] (eq. 3).

Table 3.4. Obtained fitting parameters from TDPL measurements with Varshni-Eliseev function (eq. 2).

Structure	E_0 , eV	α, meV/K	β (fixed)[48], K	σ, meV
NoAlAs-NoAnn	1.16	0.20	204	11
AlAs-NoAnn	1.19	0.13		18
AlAs-Ann	1.18	0.47		25
ThinAlAs-Ann	1.14	0.33		18

All in all, this section demonstrated that emission from Bi quantum dots can be easily tuned by controlling their size, which can be achieved by introducing additional AlAs barriers between the GaAsBi quantum well and the parabolic barrier. As a result, high structural quality dot-in-a-well structures are obtained, where the size of Bi quantum dots and thus their emission is controlled by the quantum well width. However, AlAs barriers also tend to degrade the optical performance of GaAsBi QWs. The presence of AlAs barriers leads to defect formation, resulting with lower RTPL intensity, higher carrier localization and faster intensity quenching. Fortunately, it was noticed, that *in-situ* annealing and thinning the AlAs barriers can improve optical quality of GaAsBi QWs.

Conclusions

1. Optimized thermal treatments, including high-temperature growth acting as unintentional *in-situ* annealing and subsequent *ex-situ* annealing, significantly improve structural quality, thermal stability and optical properties of GaAsBi PQW structures.
2. Thermal treatment of GaAsBi QW structures can lead to the formation of emissive Bi QDs, however structural degradation and poorly controlled size distribution may arise in the absence of sufficient suppression of interlayer Bi diffusion.
3. Ultrathin AlAs barriers effectively suppress interlayer Bi diffusion in GaAsBi/AlGaAs PQWs, improving structural uniformity and enabling controlled formation of Bi QDs within the QWs without degradation of the heterointerfaces.
4. The incorporation of AlAs barriers promotes defect-related optical degradation in GaAsBi QWs, which can be partially mitigated by *in-situ* annealing and reducing barrier thickness.

References

[1] R. D. Richards, N. J. Bailey, Y. Liu, T. B. O. Rockett, A. R. Mohmad. GaAsBi: From Molecular Beam Epitaxy Growth to Devices. Physica Status Solidi (B), **259**(2), 2100330 (2022).

[2] J. Yoshida, T. Kita, O. Wada, K. Oe. Temperature dependence of $GaAs_{1-x}Bi_x$ band gap studied by photoreflectance spectroscopy. Japanese Journal of Applied Physics, **42**, 371-374 (2003).

[3] X. Lu, D.A. Beaton, R. B. Lewis, T. Tiedje, Y. Zhang. Composition dependence of photoluminescence of $GaAs_{1-x}Bi_x$ alloys. Applied Physics Letters, **95**(4), 041903 (2009).

[4] Z. Batool, K. Hild, T. J. C. Hosea, X. Lu, T. Tiedje, S. J. Sweeney. The electronic band structure of GaAsBi/GaAs layers: influence of strain and band anti-crossing. Journal of Applied Physics, **111**(11), 113108 (2012).

[5] R. D. Richards, F. Bastiman, C. J. Hunter, D. F. Mendes, A. R. Mohmad, J. S. Roberts, J. P. R. David. Molecular beam epitaxy growth of GaAsBi using As_2 and As_4. Journal of Crystal Growth, **390**, 120–124 (2014).

[6] B. Zhang, M. Jansson, P. P. Chen, X. J. Wang, W. M. Chen, I. A. Buyanova. Effects of Bi incorporation on recombination processes in wurtzite GaBiAs nanowires. Nanotechnology, **31**, 225706 (2020).

[7] A. Štaupienė, A. Zelioli, A. Špokas, A. Vaitkevičius, B. Čechavičius, S. Stanionytė, S. Raišys, R. Butkutė, E. Dudutienė. Internal quantum efficiency of GaAsBi MQW structure for the active region of VECSELs. Applied Physics Letters, **125** (22), 221102 (2024).

[8] S. Pūkienė, M. Karaliūnas, A. Jasinskas, E. Dudutienė, B. Čechavičius, J. Devenson, R. Butkutė, A. Udal, G. Valušis. Enhancement of photoluminescence of GaAsBi quantum wells by parabolic design of AlGaAs barriers. Nanotechnology, **30**, 455001 (2019).

[9] M. Jokubauskaitė, G. Petrusevičius, A. Špokas, B. Čechavičius, E. Dudutienė, R. Butkutė. Effects of parabolic barrier design for multiple GaAsBi/AlGaAs quantum well structures. Lithuanian Journal of Physics, **63**(4), 264–272 (2023).

[10] S. Mazzucato, P. Boonpeng, H. Carrère, D. Lagarde, A. Arnoult, G. Lacoste, T. Zhang, A. Balocchi, T. Amand, X. Marie, C. Fontaine. Reduction of defect density by rapid thermal annealing in GaAsBi studied by time-resolved photoluminescence. Semiconductor Science and Technology, **28**(2), 022001 (2013).

[11] J. F. Rodrigoa, D. L. Salesa, M. Shafib, M. Heninib, L. Turyanskab, S. Novikovb, S. I. Molinaa. Effect of annealing on the structural and optical properties of (311)B GaAsBi layers. Applied Surface Science, **256**, 5688–5690 (2010).

[12] A. R. Mohmad, F. Bastiman, C. J. Hunter, R. Richards, S. J. Sweeney. Effects of rapid thermal annealing on $GaAs_{1-x}Bi_x$ alloys. Applied Physics Letters, **101**, 012106 (2012).

[13] H. Alghamdi, V. O. Gordo, M. Schmidbauer, J. F. Felix, S. Alhassan, A. Alhassni, G. A. Prando, H. Coelho-Júnior, M. Gunes, H. V. A. Galeti, Y. G. Gobato, M. Henini. Effect of thermal annealing on the optical and structural properties of (311)B and (001) GaAsBi/GaAs single quantum wells grown by MBE. Journal of Applied Physics, **127**, 125704 (2020).

[14] A. Štaupienė, M. Jokubauskaitė, A. Zelioli, A. Špokas, M. Skapas, B. Čechavičius, R. Butkutė, E. Dudutienė. Improving optical properties through growth temperatures and post-growth annealing in parabolic GaAsBi/AlGaAs quantum wells. Journal of Alloys and Compounds, **1060**, 187230 (2026).

[15] R. Butkutė, G. Niaura, E. Pozingytė, B. Čechavičius, A. Selskis, M. Skapas, V. Karpus, A. Krotkus. Bismuth Quantum Dots in Annealed GaAsBi/AlAs Quantum Wells. Nanoscale Research Letters, **12**, 436 (2017).

[16] R. Butkutė, M. Skapas, A. Selskis, V. Bukauskas, S. Stanionytė, and G. Niaura. AlAs as a Bi blocking barrier in GaAsBi multi-quantum wells: structural analysis. Lithuanian Journal of Physics, **57**(1), 29–36 (2017).

[17] A. Vaitkevičius, A. Špokas, A. Zelioli, U. Cibulskaitė, A. Bičiūnas, E. Dudutienė, B. Čechavičius, M. Skapas, A. Čerškus, M. Talaikis, P. Baranowski, P. Wojnar, R. Butkutė. Segregation-driven formation of bismuth quantum dots in parabolic GaAsBi/AlGaAs quantum structures. Surfaces and Interfaces, **68**, 106586 (2025).

[18] M. Skapas, E. Luna, S. Stanionytė, K. Graser, R. Butkutė. In Situ TEM Study of Size-Controlled Bi Quantum Dots in an Annealed GaAsBi/AlAs Multiple Quantum Well Structure. ACS Omega, **10** (10), 10432-10437 (2025).

[19] K. Alberi, J. Wu, W. Walukiewicz, K. M. Yu, O. D. Dubon, S. P. Watkins, C. X. Wang, X. Liu, Y. J. Cho, J. Furdyna. Valence-band anticrossing in mismatched III-V semiconductor alloys. Physical Review B, **75**, 045203 (2007).

[20] M. Usman, C. A. Broderick, A. Lindsay, E.P. O'Reilly. Tight-binding analysis of the electronic structure of dilute bismide alloys of GaP and GaAs. Physical Review B, **84**, 245202 (2011).

[21] A. F. Phillips, S. J. Sweeney, A. R. Adams, P. J. A. Thijs. Compressively Strained InGaAs(P) MQW Semiconductor Lasers. IEEE Journal of Selected Topics in Quantum Electronics, **5**(3), 401–412 (1999).

[22] X. Wu, W. Pan, Z. Zhang, Y. Li, C. Cao, J. Liu, L. Zhang, Y. Song, H. Ou, S. Wang. 1.142 μm GaAsBi/GaAs Quantum Well Lasers Grown by Molecular Beam Epitaxy. ACS Photonics, **4**(6), 1322– 1326 (2017).

[23] T. Fuyuki, R. Yoshioka, K. Yoshida, M. Yoshimoto. GaAsBi Laser Diodes with Low Temperature Dependence of Lasing Wavelength. CLEO, 1-2 (2014).

[24] Y. Tominaga, K. Oe, M. Yoshimoto. Low temperature dependence of oscillation wavelength in $GaAs_{1-x}Bi_x$ laser by photo-pumping. Applied Physics Express, **3**, 062201 (2010).

[25] R. B. Lewis, D. A. Beaton, X. Lu, T. Tiedje. $GaAs_{1-x}Bi_x$ light emitting diodes. Journal of Crystal Growth, **311**, 1872–1875 (2009).

[26] P. Ludewig, N. Knaub, N. Hossain, S. Reinhard, L. Nattermann, I.P. Marko. Electrical injection Ga(AsBi)/(AlGa)As single quantum well laser. Applied Physics Letters, **102**(24), 242115 (2013).

[27] R. Butkutė, A. Krotkus, V. Pačebutas, V. Bukauskas, A. Geižutis, P. Ludewig, B. Čechavičius, R. Kundrotas, K. Volz. Multi-quantum well Ga(AsBi)/GaAs laser diodes with more than 6% of bismuth. Electronics Letters, **50**, 1155–1157 (2014).

[28] J. Puustinen, J. Hilska, M. Guina. Analysis of GaAsBi growth regimes in high resolution with respect to As/Ga ratio using stationary MBE growth. Journal of Crystal Growth, **511**, 33-41 (2019).

[29] P. K. Patil, F. Ishikawa, S. Shimomura. GaAsBi/GaAs MQWs grown by MBE using a two-substrate-temperature technique. Journal of Alloys and Compounds, **725**, 694-699 (2017).

[30] E. Dudutienė, A. Jasinskas, S. Stanionytė, M. Skapas, A. Vaitkevičius, B. Čechavičius, R. Butkutė. Impact of elevated GaAs barrier growth temperature on the homogeneity and photoluminescence of GaAsBi multiple quantum wells. Materials Science in Semiconductor Processing, **199**, 109828 (2025).

[31] A. Špokas, A. Zelioli, A. Biciunas, B. Čechavičius, J. Glemža, S. Pralgauskaitė, M. Kamarauskas, V. Bukauskas, J. Spigulis, Y. J. Chiu, J. Matukas, R. Butkutė. Optimising (Al,Ga) (As,Bi) Quantum Well Laser Structures for Reflectance Mode Pulse Oximetry. Micromachines, **16**, 506 (2025).

[32] L. Gelczuk, J. Kopaczek, D. Pucicki, T. B.O. Rockett, R. D. Richards, R. Kudrawiec. Effects of rapid thermal annealing on deep-level defects and optical properties of n-type GaAsBi alloys grown by molecular beam epitaxy at low temperature. Materials Science in Semiconductor Processing, **169**, 107888 (2024).

[33] V. Pačebutas, R. Butkutė, B. Čechavičius, S. Stanionytė, E. Pozingytė, M. Skapas, A. Selskis, A. Geižutis, A. Krotkus. Bismides: 2D structures and quantum dots. Journal of Physics D: Applied Physics, **50**, 36 (2017).

[34] F. Franchello, L. D. Souza, E. Laureto, A. A. Quivy, I. F.L. Dias, J. L. Duarte. Influence of bimodal distribution and excited state emission on photoluminescence spectra of InAs self-assembled quantum dots. Journal of Luminescence, **137**, 22-27 (2013).

[35] M. Bennour, L. Bouzaiene, F. Saidi, L. Sfaxi, H. Maaref. Abnormal temperature dependencies of photoluminescence and carrier transfer in InAs QDs and DWELL structures grown on GaAs (115)A emitting near 1.3µm wavelength. Journal of Luminescence, **148**, 207-213 (2014).

[36] E. Dudutienė, A. Jasinskas, B. Čechavičius, R. Nedzinskas, M. Jokubauskaitė, A. Bičiūnas, V. Bukauskas, G. Valušis, and R. Butkutė. Photoluminescence properties of GaAsBi single quantum wells with 10% of Bi. Lithuanian Journal of Physics, **61**, 142–150 (2021).

[37] T. Lu, Z. Ma, C. Du, Y. Fang, H. Wu, Y. Jiang, L. Wang, L. Dai, H. Jia, W. Liu, H. Chen. Temperature-dependent photoluminescence in light-emitting diodes. Scientific Reports, **4**, 6131 (2014).

[38] J. B. Herzog. Optical spectroscopy of colloidal CdSe semi-conductor nanostructures. University of Notre Dame, Thesis, (2011).

[39] M. P. Polak, P. Scharoch, R. Kudrawiec. First-principles calculations of bismuth induced changes in the band structure of dilute Ga-V-Bi and In-V-Bi alloys: Chemical trends versus experimental data. Semiconductor Science and Technology, **30**(9), 094001 (2015).

[40] T. Wilson, N. P. Hylton, Y. Harada, P. Pearce, D. Alonso-Álvarez, A. Mellor, R. D. Richards, J. P. R. David, N. J. Ekins-Daukes. Assessing the Nature of the Distribution of Localised States in Bulk GaAsBi. Scientific Reports, **8**, 6457 (2018).

[41] N. Tucher. Analysis of photonic structures for silicon solar cells. Fraunhofer Institute for Solar Energy Systems ISE, Thesis, (2016).

[42] M. A. Reshchikov. Measurement and analysis of photoluminescence in GaN. Journal of Applied Physics, **129**(12), 121101 (2021).

[43] E. Luna, J. Puustinen, J. Hilska, M. Guina. Detection of BiGa hetero-antisites at Ga(As,Bi)/(Al,Ga)As interfaces. Journal of Applied Physics, **135**(12), 125303 (2024).

[44] T. Schmidt, K. Lischka, W. Zulehner. Excitation-power dependence of the near-band-edge photoluminescence of semiconductors. Physical Review B, **45**(16), (1992).

[45] I. Moussa, H. Fitouri, Z. Chine, A. Rebey, B. El Jani. Effect of thermal annealing on structural and optical properties of the $GaAs_{0.963}Bi_{0.037}$ alloy. Semiconductor Science and Technology, **23**(12), (2008).

[46] H. Makhloufi, P. Boonpeng, S. Mazzucato, J. Nicolai, A. Arnoult, T. Hungria, G. Lacoste, C. Gatel, A. Ponchet, H. Carrere, X. Marie, C. Fontaine. Molecular beam epitaxy and properties of GaAsBi/GaAs quantum wells grown by molecular beam epitaxy: effect of thermal annealing. Nanoscale Research Letters, **9**(1), 123 (2014).

[47] P. G. Eliseev, P. Perlin, J. Lee and M. Osiński. " respectively " temperature induced shift and band-tail emission in InGaN-based light sources. Applied Physics Letters, **71**, 569 (1998).

[48] I. Vurgaftman, J. R. Meyer, L. R. Ram-Mohan. Band parameters for III-V compound semiconductors and their alloys. Journal of Applied Physics, **89**, 5815-5875 (2001).

[49] R. Chen, H. Y. Liu, H. D. Sun. Electronic energy levels and carrier dynamics in InAs/InGaAs dots-in-a-well structure investigated by optical spectroscopy. Journal of Applied Physics, **107**, 013513 (2010).

[50] D. I. Lubyshev, P.P. Gonzalez-Borrero, E. Marega, Jr., E. Petitprez, N. La Scala, Jr., P. Basmaji. Exciton localization and temperature stability in self-organized InAs quantum dots. Applied Physics Letters, **68**, 205 (1996).

[51] J. C. Lee. Temperature dependence of the spontaneous emission mechanisms of localized-state heterosystem. Optica Applicata, **41**(4), (2011).

[52] R. Heitz, F. Guffarth, I. Mukhametzhanov, M. Grundmann, A. Madhukar, D. Bimberg. Many-body effects on the optical spectra of InAs/GaAs quantum dots. Physical Review B, **62**(24), 16881 (2000).

[53] E. C. Le Ru, J. Fack, R. Murray, Phys. Rev. B 67 (2003), 245318. R. Jawher, M. Oueslati, V. Sallet, J. Harmand, R. Chtourou, An explanation for the non-monotonic temperature dependence of the photoluminescence spectral features of self-organized InAs QDs. Journal of Luminescence, **253**, 119441 (2023).

[54] T. V. Torchynska, J. L. Casas Espinola, L. V. Borkovska, S. Ostapenko, M. Dybiec, O. Polupan, N. O. Korsunska, A. Stintz, P. G. Eliseev, K. J. Malloy. Thermal activation of excitons in asymmetric InAs dots-in-a-well $In_xGa_{1-x}As/GaAs$ structures. Journal of Applied Physics, **101**, 024323 (2007).

[55] M. Wu, E. Luna, J. Puustinen, M. Guina, A. Trampert. Formation and phase transformation of Bi containing QD-like clusters in annealed GaAsBi. Nanotechnology, **25**, 205605 (2014).

[56] J. Puustinen, M. Wu, E. Luna, A. Schramm, P. Laukkanen, M. Laitinen, T. Sajavaara, M. Guina. Variation of lattice constant and cluster formation in GaAsBi. Journal of Applied Physics, **114**, 243504 (2013).

[57] T. Hepp, J. Veletas, R. Günkel, O. Maßmeyer, J. Glowatzki, W. Stolz, S. Chatterjee, K. Volz. Dilute Bismuth Containing W-Type Heterostructures for Long-Wavelength Emission on GaAs Substrates. Crystal Growth & Design, **21**(11), 6307 (2021).

[58] M. Jiang, H. Xiao, S. Peng, L. Qiao, G. Yang, Z. Liu, X. Zu. First-Principles Study of Point Defects in GaAs/AlAs Superlattice: the Phase Stability and the Effects on the Band Structure and Carrier Mobility. Nanoscale Research Letters, **13**, 301 (2018).

Summary

OPTICAL INVESTIGATION OF ANNEALED GaAsBi/AlGaAs PARABOLIC QUANTUM WELLS WITH Bi QUANTUM DOTS

Aistė Štaupienė

GaAsBi quantum well (QW) structures are one category of materials currently being studied as an active area for light sources operating in the near-infrared range. GaAsBi exhibits a low temperature sensitivity of the bandgap energy, a pronounced bandgap reduction with increasing bismuth incorporation and the potential to suppress non-radiative Auger recombination mechanisms. However, the growth of GaAsBi quantum structures with high emission efficiency is challenging. Bi incorporation into the GaAs lattice requires very low growth temperatures, which lead to a high defect concentration in the structures. In order to increase the photoluminescence (PL) intensity of GaAsBi QWs, various technological approaches are employed: the use of graded AlGaAs barriers improves carrier confinement and trapping efficiency, while annealing reduces the defect concentration. At the same time, thermal treatments can promote Bi segregation, which may lead to the formation of Bi quantum dots (QDs). To control the size of Bi QDs and to avoid structural degradation caused by enhanced Bi migration, ultrathin AlAs layers can be used as Bi-blocking barriers. The aim of this work was to investigate how annealing and barrier design affect optical and structural properties of GaAsBi/AlGaAs parabolic quantum wells (PQWs) with Bi QDs.

In the first part of the thesis, *in-situ* and *ex-situ* annealed GaAsBi PQW structures were studied. Analysis of transmission electron microscopy micrographs showed that *in-situ* annealing improved structural quality, while PL measurements revealed reduced non-radiative recombination, enhancing the emission intensity and reducing thermal PL quenching. For the e*x-situ* annealing, samples were thermally treated in a rapid thermal annealing (RTA) furnace at 650 °C, 700 °C and 750 °C. It was found that the optimal RTA temperature was structure-dependent: previously *in-situ* annealed structure exhibited higher thermal stability and could benefit from higher RTA temperatures before the signs of degradation appeared.

In the second part of this work, Bi redistribution and cluster formation induced by annealing treatments were investigated. It was shown that insufficient suppression of interlayer Bi diffusion leads to distortion of the QW structure and formation of Bi QDs. PL measurements revealed a broad emission band and a S-shaped temperature dependence of the PL peak, associated with carrier localization in Bi QDs of different sizes. In contrast, by introducing ultrathin AlAs layers and thereby effectively suppressing Bi diffusion, it becomes possible to control the size of formed QDs and tune their emission. In such structure, a narrow cathodoluminescence band at ~ 0.9 eV was observed and attributed to emission from Bi QDs with a size comparable to the QW width.

In the third part of the thesis, the effect of additional ultrathin AlAs barrier layers on emission from GaAsBi QWs was investigated. It was found that introduction of AlAs barriers degrades the optical quality of the samples by defect formation. Structures containing AlAs barriers had stronger carrier localization, faster thermal PL quenching and overall weaker emission intensity. Fortunately, it was shown that these optical properties can be improved by reducing AlAs barrier thickness and employing additional *in-situ* annealing.

Thus, this work demonstrates that annealing and barrier design strongly affect the optical properties of GaAsBi PQWs. Optimized annealing significantly enhances emission from GaAsBi QWs and promotes Bi QD formation, while Al-containing barriers enable control over the size of these QDs and their emission wavelength.

Santrauka

ATKAITINTŲ GaAsBi/AlGaAs PARABOLINIŲ KVANTINIŲ DUOBIŲ SU SUSIFORMAVUSIAIS Bi KVANTINIAIS TAŠKAIS OPTINIS TYRIMAS

Aistė Štaupienė

GaAsBi kvantinės struktūros yra perspektyvi medžiaga aktyviajai artimosios infraraudonosios spinduliuotės šaltinių sričiai. Bismidų draustinių energijų tarpas silpnai kinta nuo temperatūros, o įterpus vos kelis procentus Bi į GaAs gardelę galima ženkliai paslinkti GaAsBi optinį atsaką į ilgesnių bangų sritį. Tačiau GaAsBi kvantines struktūras, pasižyminčias dideliu fotoliuminescencijos (PL) efektyvumu, užauginti yra sudėtinga, nes Bi įterpimui į GaAs reikalingos labai žemos auginimo temperatūros, kurios lemia didelę defektų koncentraciją bandiniuose. Siekiant padidinti GaAsBi kvantinių duobių (QW) emisijos intensyvumą, taikomi įvairūs technologiniai metodai. Pavyzdžiui, gradientinių AlGaAs barjerų panaudojimas padidina krūvininkų pagavimo efektyvumą, o struktūrų atkaitinimas sumažina defektų koncentraciją. Pakelta temperatūra tuo pačiu skatina ir Bi atomų difuziją, dėl kurios gali susiformuoti Bi kvantiniai taškai (QDs). Siekiant kontroliuoti šių Bi QDs dydį ir išvengti kvantinės struktūros deformacijos dėl padidėjusios Bi segregacijos, gali būti naudojami itin ploni AlAs sluoksniai, veikiantys kaip Bi difuziją blokuojantys barjerai. Šio darbo tikslas – ištirti, kaip struktūrų atkaitinimas bei jų barjero dizainas veikia GaAsBi/AlGaAs parabolinių kvantinių duobių (PQW) su Bi QDs emisiją ir struktūrines savybes.

Pirmoje darbo dalyje buvo tiriamos *in-situ* bei *ex-situ* atkaitintos GaAsBi PQW struktūros. Peršviečiamosios elektroninės mikroskopijos nuotraukų analizė parodė, kad *in-situ* atkaitinimas lėmė geresnę bandinių struktūrinę kokybę, o PL matavimai atskleidė, jog dėl atkaitinimo sumažėjo nespindulinė rekombinacija, kas lėmė, jog išaugo emisijos intensyvumas bei sumažėjo temperatūrinis PL intensyvumo kritimas. Papildomai struktūras atkaitinus greito atkaitinimo krosnyje (RTA) 650 °C, 700 °C bei 750 °C temperatūrose (*ex-situ*), nustatyta, jog optimali RTA temperatūra priklauso nuo tiriamos struktūros: auginimo metu atkaitinta struktūra pasižymėjo didesniu terminiu stabilumu, išlaikydama bei pagerindama savo optines savybes esant aukštesnėms RTA temperatūroms.

Antroje darbo dalyje buvo tiriamas atkaitinimo metu vykstantis Bi persiskirstymas ir Bi nanokristalitų formavimasis GaAsBi PQW struktūrose. Parodyta, jog esant nepakankamam tarpsluoksninės Bi difuzijos blokavimui susiformuoja netvarki DWELL (ang. *Dot-in-a-Well*) struktūra, kurios PL matavimuose stebima plati emisijos juosta bei S-formos temperatūrinis PL smailės kitimas, siejamas su krūvininkų lokalizacija skirtingo dydžio Bi QDs. Tuo tarpu efektyviai ribojant Bi difuziją, pavyzdžiui, pasitelkus itin plonus AlAs sluoksnius, galima kontroliuoti susiformuojančių QDs dydį bei taip valdyti jų emisiją. Tokioje struktūroje 10 K temperatūroje gauta siaura

katodoliuminescencijos juosta ties ~ 0,9 eV buvo priskirta emisijai iš Bi QDs, kurių dydis buvo artimas kvantinės duobės storiui.

Trečioje darbo dalyje buvo tiriama papildomų itin siaurų AlAs barjerinių sluoksnių įtaka emisijai iš GaAsBi QWs. Nustatyta, jog AlAs barjerai pablogina optinę bandinių kokybę. PL matavimai parodė, kad tirtose struktūrose pasireiškė krūvininkų lokalizacija, kuri stiprėjo didėjant AlAs barjerų storiui. Atitinkamai, temperatūrinis PL intensyvumo kritimas buvo lėčiausias struktūroje be AlAs barjerų ir greitėjo didėjant AlAs barjerų storiui. Didžiausias PL intensyvumas kambario temperatūroje buvo stebimas bandinyje be AlAs barjerų, o silpniausias – struktūrose su storesniais AlAs barjerais. Vis dėl to buvo nustatyta, kad GAAsBi QW optines savybes galima pagerinti naudojant plonesnius AlAs barjerus bei papildomai taikant *in-situ* struktūrų atkaitinimą.

Taigi, gauti rezultatai leidžia teigti, jog struktūrų atkaitinimas bei jų barjero dizainas stipriai veikia GaAsBi PQW optines savybes: optimizuotas atkaitinimas pagerina emisiją iš GaAsBi QWs bei skatina Bi QDs formavimąsi, o Al turintys barjerai leidžia kontroliuoti šių kvantinių taškų dydį bei emisijos bangos ilgį.